Advanced Dispatching of a Wind Farm Based on Doubly Fed Induction Generators for the Improvement of LVRT Capability by the ADRC Approach

Hammadi LAGHRIDAT [1], *Ahmed ESSADKI* [1], *Tamou NASSER* [2]

[1]Electrical Laboratory Research, Higher National School of Arts and Crafts, Mohammed V University, Avenue des Nations Unies, Agdal, 10106 Rabat, Morocco.
[2]Electrical Laboratory Research, National High School for Computer Science and Systems, Mohammed V University, Avenue des Nations Unies, Agdal, 10106 Rabat, Morocco.

hammadi.laghridat@um5s.net.ma, ahmed.essadki1@gmail.com, tamounasser@gmail.com

DOI: 10.15598/aeee.v20i4.4411

Article history: Received Nov 13, 2021; Revised Feb 08, 2022; Accepted Apr 03, 2022; Published Dec 31, 2022.

Abstract. *This paper aims to explore a viable monitoring and management of active and reactive powers for a large-scale wind farm based on Doubly-Fed Induction Generators (DFIG) considering the voltage Fault-Ride-Through capability (FRT), especially Low-Voltage-Ride-Through (LVRT) capability by using a new control strategy, known as Active Disturbance Rejection Control. This strategy uses real-time estimation and compensation of the generalized "total" disturbance before it affects the system. The wind farm supervisory unit is used to coordinate the control of the powers production by the entire wind farm, which must take into account the couplings between each wind generator while producing the individual power commands. The turbine control units (local supervisory units) send the appropriate power references depending on the situation. This can be to produce the maximum power, to manage the active and reactive power given by the Transmission System Operator (TSO) or to meet the requirements of the grid code (LVRT capacity). However, to ensure the dispatching of the references of the active and reactive powers over the all wind generators of the wind farm and to satisfy the security of the power grid, we utilized mean of the proportional distribution algorithm.*

The effectiveness of the proposed supervisory approach and control strategies are tested and validated through a multiples scenarios of simulations that are made under the MATLAB/Simulink Environment. The results obtained have demonstrated the efficiency and robustness of the control methods, and also the fact that they guarantee good performance and safety of the integration of wind farms into the grid while complying with the requirements of the grid code during power system faults.

Keywords

Wind Farm, Wind Generator, Supervisory, DFIG, LVRT, ADRC.

1. Introduction

Wind power is a Renewable and a clean Energy Source (RES), and it is considered as rapid rising energy resource in the worldwide with an average growth rate of 30 %. Due to its advantages in terms of substantial potential and mature technology and the distribution reserves, related studies and infrastructure construction for the global utilization are being developed rapidly. Moreover, the recent development of power electronics systems and a great transformation in power system industry have reflected positively on the wind turbines technology. The capacity of global wind power has reached 433 GW in 2015 and is expected to exceed 792 GW by 2020 [1] as shown in Fig. 1. In 2015, China has the biggest market in the wind power industry [2], while in Europe, the wind

energy has also reached a very high level of the integration in the power system. According to Wind-Europe's Central Scenario, the Denmark was the country that used the most wind power in its energy demand last year (48 %), followed by Ireland (33 %) and Portugal (27 %) [3].

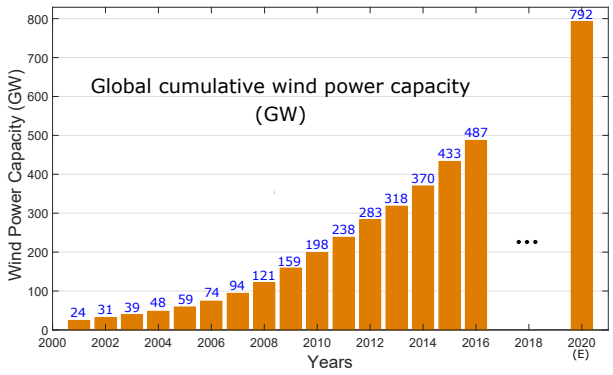

Fig. 1: Global cumulative wind power capacity from 2001 to 2020 [1].

Nowadays, the DFIG based Wind Farms (WFs) are the most important sources of wind power and has been largely utilized in large-scale electricity generation, due to its prominent advantages such as its ability of high output power [4], high electromechanical efficiency, improved power quality, high power capturing, wide range of speed variation, reduced mechanical stress on turbine, and the flexibility for controlling independently the active and reactive powers. In addition, it operates with three-phase bidirectional power electronic converters that have less power capacity than the full power rating, which is typically about 30 %, compared to the full power rating converter configurations that are used in wind farms based on Squirrel-Cage Induction Generators (SCIGs) [5] or Permanent Magnet Synchronous Generators (PMSGs) [6], which reducing costs and losses in wind turbine systems. In this structure, the stator windings of the DFIG are directly interconnected to the power network and its rotor windings are interconnected by using of a bidirectional three phase power electronics converters, which are called the Grid Side Converter (GSC) and Rotor Side Converter (RSC). In contrast, despite the benefits of DFIG-based wind turbine over the other configurations of wind generators (SCIG and PMSG), the DFIG-based WFs are more sensitive to voltage dips and grid disturbances, wherein the dynamic performances of the WFs becomes unstable and more complicated and poses many challenges to the grid.

No electrical network is immune to short, unwanted and random disturbances such as voltage dips. This type of disturbance is inevitably an integral part of the operation of a power system and it is obvious that its proper management and regular maintenance reduces the risk of disturbance. However, during the voltage dip, high transient overcurrents appear in the DFIG rotor circuit and flow through the power electronics converters, these overcurrents may exceed the maximum fault current tolerated by the converter's semiconductors, which can damage the DFIG's converters or either trip out the WTs [7]. As a result, the generator's mechanical speed becomes excessively high and finally, the system loses its stability. Therefore, the DFIG-based WT cannot operate properly during the fault without any protection system. In order to overcome these problems, a protection system is required to ensure the security of the power system and meet certain requirements of connection to the power grid, which are commonly defined as Grid Codes (GCs). Those requirements require the wind generator to remain connected and continue the production of electricity during the faults; this process is known as the Low Voltage Ride Through (LVRT) capability.

Because of the unforeseeable nature of their primary source of power, the integration of DFIG based wind farms with a large capacity to the power grid has engendered some challenges to the TSO. These include, for example, the stability of the electrical power system and the electrical system reliability and power quality, and also the regulation of voltage and frequency [8]. The large-scale wind farm usually contains dozens to hundreds of wind generators interconnected to the electrical network at the Point of Common Coupling (PCC). It is usually monitored to provide the maximum wind power, to ensure the reactive power and active powers demand by the network operator and to satisfy the Grid Code Requirement (GCR). Depending on the actual power system situation and the control mode requested by the TSO (hourly generation required), the WF's Central Supervisory Unit (CSU) is configured to control and monitor the total reactive and active powers exchanged with the electrical grid, in operating modes such as optimal power control (maximum power point tracking), fault control or PQ control. Besides this, the Local Supervision Unit (LSU) of each WT is designed to estimate the maximum power capacity and to gather and forward the relevant WTs pieces of information to the CSU. [9]. Thus, to optimally distribute the powers production between the different WTs, one must take into consideration the reliable operation and the security of the wind farm. In literature, several techniques have been investigated for the conception of the supervisory algorithms for wind farms. In Overall, the supervisory algorithms may be split into three categories: supervisory algorithms on the basis of proportional-integral PI controllers; supervisory algorithms based on optimization functions, and supervisory algorithms based on a proportional distribution.

For the supervisory algorithms based on PI controllers, we can distinguish two types which the first use the PI controller to set the power factor of WF as have been proposed in the literature [8] and [9]. The second type regulates directly the active and reactive powers of WF, see [10] and [11]. Moreover, for the supervisory algorithms based on OFs, several researchers have concentrated on the monitoring of the reactive and active powers of the WF to minimize its losses. In [12], the minimum cable losses as the optimal objective is proposed. The authors in [13], focus on minimizing the sum of transformer and cable losses. In [14], the authors proposed a strategy for reactive power allocation for the DFIG based WF with loss minimization. Additionally, the supervisory control based on Proportional Distribution (PD) algorithm was developed in [15] and [16], where the main objective is to dispatch the power proportionally on the farm wind generators. The comparison between these three algorithms from a safety point of view and the risk of wind generators saturation have shown that the PD algorithm guarantees that each of the wind generators will always operate far from its (P,Q) diagram limits. For the improvement of the wind turbines power control, and to overcome the shortcomings of classic controllers such as PID, RST controllers, we have used in this paper a Novel ADRC control approach. This controller allows a very good elimination of the disturbances in real time which can be numerous on such wind system, given the complexity and the number of sensors involved. It also allows to meet the robustness requirements against the variations of the system parameters and the uncertainties of its mathematical model [6]. In this context, ADRC has been largely used in different areas, like wind power generation systems with different variable-speed wind turbine technologies. In our previous article [17], we have presented the control by ADRC to reject the internal disturbances of DFIG-based wind turbine in order to investigate the real-time behavior and sensitivity of the DFIG controllers to the variation of the parameters. As a result, we have proposed this approach in this research article to enhance the rejection of the network disturbances and to enhance LVRT capability.

In this this research article, we have two main contributions. The first is the control of active and reactive power for a wind turbine at PCC with a novel control structure by the ADRC Strategy. The second lies in dispatching and controlling of the output powers of the wind farm in order to satisfy the grid code requirements while considering the Low Voltage Ride-through capability. Moreover, to ensure the interactions between the wind turbines generators. As a result, this article is structured as follows, it is dived into seven sections, where in Sec. 2. , the FRT and LVRT Capability Regulations for Various Grid Codes is presented. In Sec. 3. , the architecture and Modeling of aggregated DFIG wind farm is designed. The mathematical Theory of the ADRC Method is presented in Sec. 4. The control of DFIG-based WT by ADRC strategy is treated in Sec. 5. The Sec. 6. deals with the supervisory system of the wind farm. Finally, the Sec. 7. presents the validation and the simulation results.

2. FRT/LVRT Capability Regulations for Various Grid Codes

2.1. Fault Ride-Through Capability Enhancement of DFIG-based WTs

Fast growth of large wind farms using DFIG has resulted in the setting of new grid codes, wherein the primary requirements are the ability of wind generators to withstand the LVRT and FRT. The major aim was to ensure that wind turbines withstand voltage drops at the PCC and stay connected to the power grid to support the voltage throughout and beyond the fault. In addition, voltage drop can be caused by many different reasons, the most famous of which is a short circuit affecting the network or connected installations with high currents such as the starting of high power motors, transformers, electric arcs and the disconnection of capacitive loads or production installations.

Over the past decades, several strategies have been investigated to improve the FRT capability of the WT. These techniques can be classified into two types: Hardware strategies and software strategies. In addition, hardware strategies can be classified into two main solutions (Fig. 2), the solutions based on hardware strategies using storage-based methods and protection circuits such as the crowbar method, in which the literature [18], [19] and [20] has proposed the use of crowbar with a series braking resistor, with a series R-L and with a DC link chopper respectively. The second hardware solution is the Energy Storage Method (ESM) is discussed in [21]. The other hardware solutions which are based on Series Grid Side Converter (SGSC) and Series Dynamic Breaking Resister (SDBR) were proposed and investigated in the literature [22] and [23] respectively. The last hardware solution method is based on Fault Current Limiter (FCL), see [24] and [25]. In these works, the authors presented a Non-controlled Fault Current Limiter (NC-FCL) and Superconducting Fault Current Limiter (SFCL) to improve FRT capability of DFIG-based wind turbine. In contrast, the solutions based on hard-

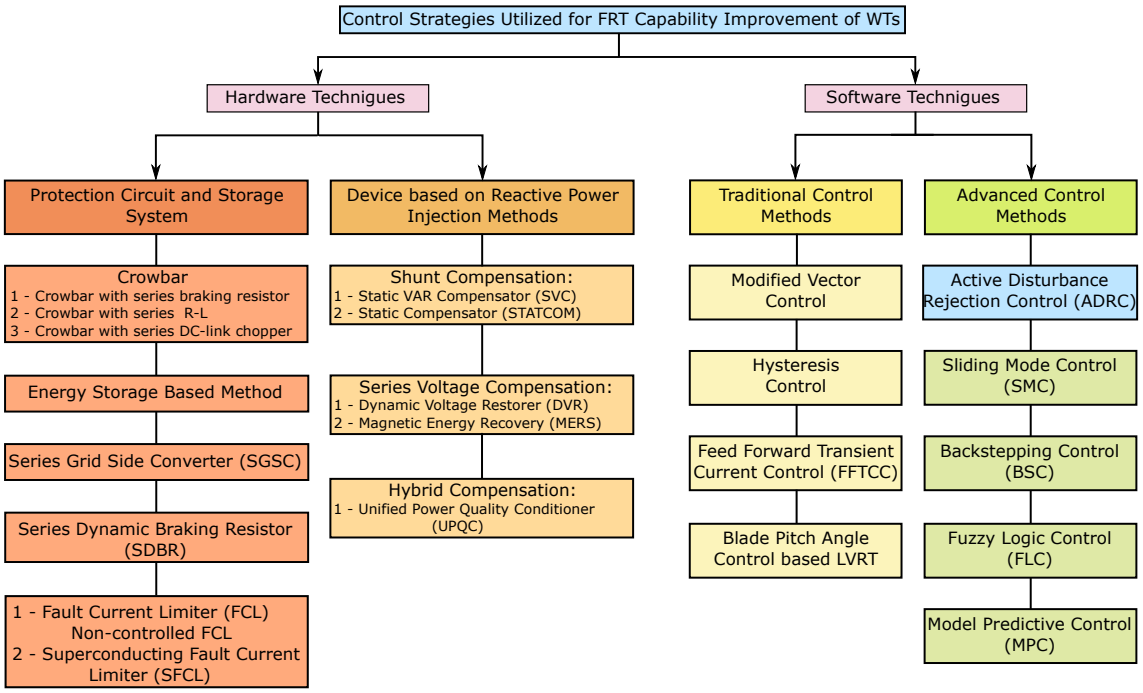

Fig. 2: Strategies for improving the FRT capability of WTs.

ware strategies using Devices based on reactive power injection methods such as a Static VAR Compensator (SVC) and Static Compensator (STATCOM) are discussed in [26] and [27], the works of literature [28] and [29] proposes the use of the Dynamic Voltage Restorer (DVR) and Magnetic Energy Recovery (MERS) methods to Improve FRT Capability of DFIG-Based WTs, in addition, the Unified Power Quality Conditioner (UPQC) method can improve the FRT capability as have been studied in the work [30].

In opposition to hardware strategies, the software strategies do not use external devices based FRT techniques of WT, they are based on internal control modifications in the RSC and GSC, which are further subdivided into traditional control methods and advanced control methods. The solutions based on traditional control methods such as, a modified vector control, have been proposed in [31]. The works of literature [32] and [33] have presented respectively, the Hysteresis Control and the Feed forward Transient Current Control (FFTCC) utilized for FRT capability improvement of WTs. Moreover, there are old methods based on blade pitch angle control, see [34]. Fortunately recently, wind turbines control has been developed and this has reflected positively the enhancement of the voltage drops problems. Several solutions based on advanced control methods have been also presented in the literature. For example, in [35], the authors proposed an FRT capability enhancement method for the DFIG based WT by using Sliding Mode Control (SMC). The literature [36] and [37] proposed and studied the Backstepping Control (BSC) and Fuzzy Logic Control (FLC) for WTs during various fault conditions, respectively. Moreover, in [38], the authors presented a method to meet low-voltage ride-through requirements using a Model Predictive Control (MPC). Figure 2 summarizes the control strategies utilized for FRT capability improvement of WTs.

2.2. LVRT Capability Regulations for Various Grid Codes

In order to ensure a secure and reliable supply of electricity with integrated wind power plants, large-scale wind farms must meet certain requirements of connection to the power grid, which are commonly defined as Grid Codes (GCs). The problem of grid code requirements for large WF has been already investigated in several research works, but in [39] the author presented a review of international GCs of various countries for wind power integration. The European countries have developed a specific grid code for wind power plants interconnected at Medium (MV) and High Voltage (HV) power grids. These specifications vary between countries and depend on the robustness of the national or regional power network, Fig. 3(a) presents the LVRT grid code requirements for different countries.

Different GCs regulations for LVRT enhancement are summarized as follows:

- Wind generators must remain connected to the power grid for a predetermined period of time

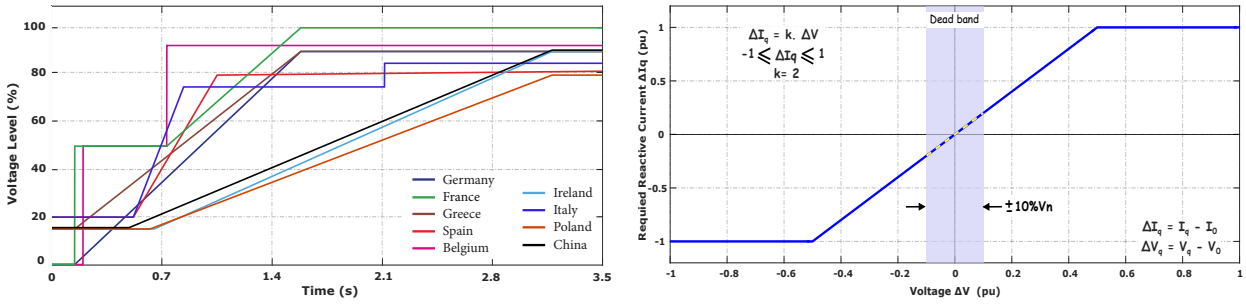

(a) (b)

Fig. 3: German GC Regulations: (a) The profile of voltage drop (LVRT), (b) Reactive current requirement. [16]

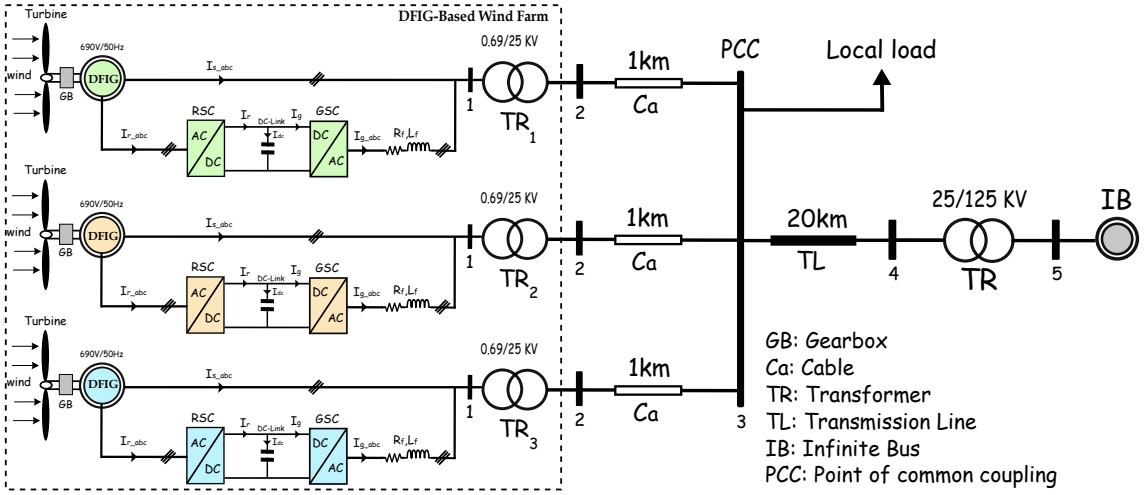

Fig. 4: Architecture of wind farm aggregated DFIG.

for a certain range of voltage drops at the PCC. For example, the voltage-time curves for Germany, Spain, Belgium, Ireland, Italy, Poland, China, and Greece are shown in Fig. 3(a), it can be observed that the wind generator has to stay attached to the network during failures in the areas located below the curves. Moreover, IEC 61400-21 also specifies the voltage dips tests for wind generators in order to check their responsiveness to the power network voltage drops [40].

- Wind generators must provide a given quantity of reactive power (reactive current) to support the network voltage stability within the fault. Figure 3(b) demonstrates the German GC requirements of reactive current. It is shown in this figure that each percent of voltage drop requires a 2 % of the reactive current injection for the voltage dips from 10 % up to 50 %. When the voltage dip value is higher than 50 %, the injection of reactive current goes to 100 % of the rated current.

3. Architecture and Modeling of Aggregated DFIG Wind Farm

The proposed wind farm architecture is depicted in Fig. 4, it consists of three chains that contain a wind turbine using a DFIG generator that is directly connected to the grid via the stator side and indirectly via the rotor side using a bidirectional RSC and GSC converters. The connection between the wind turbine generators and the power grid is insured by cables at PCC and the overhead transmission line with the step-up transformers whether 0.69/25 kV or 25/125 kV, the nominal power capacity for each wind turbine generator is about 1.5 MW.

To demonstrate the supervisory and the wind turbine advanced control strategy, the model of DFIG-based wind farm is given is this section. In addition, the wind turbine detailed model is composed of a three-bladed rotor, a mechanical gearbox, an electrical generator (DFIG) with the bidirectional RSC and GSC converters, DC-Link capacitor, and the line filter.

The wind's kinetic energy is captured by the WT system and then converted into mechanical energy which rotates the rotors-blades, the DFIG converts this mechanical power to a variable electrical power and it is subsequently injected into the grid. The DFIG-based WT reactive and active powers can be controlled independently through rotor side and grid side controls. However, to further study the proposed system performances, we began by the modelling in the dq-synchronous reference. The power system data is summarized in Appendix 1.1.

3.1. Wind Power Dynamic Model

The WT system dynamic model has been discussed in several different works [4], [5] and [6], which we will briefly present. Wherein, the aerodynamic power extracted from the wind can be expressed by the Eq. 1, which it's depends on the aerodynamic behavior of each wind turbine.

$$P_{aero\_i} = C_p(\lambda\_i, \beta\_i) P_{w\_i}, \tag{1}$$

$$P_{aero\_i} = C_p(\lambda\_i, \beta\_i)\ \frac{1}{2}\ \rho\ A_{wt\_i}\ {w_t}_{\_i}^{3}\ , \tag{2}$$

where C_p is the power coefficients; P_w is the wind's kinetic power; A_{wt_i}, ρ and ${w_t}_{\_i}$ are the turbine blades area, the air density and the wind velocity of the wind turbine i^{th}, respectively. The expression of the tip speed ratio is defined as:

$$\lambda\_i = \frac{R\ \Omega_{tur\_i}}{{w_t}_{\_i}}, \tag{3}$$

where Ω_{tur_i} and R are the rotational speed and the blades radius of the turbine, respectively.

The Fig. 5 represents the aerodynamic power of the WTs according to λ_i and the wind velocity. We notice that the maximum power is 1.5 MW when the wind velocity is equal to 12 m· s^{-1} (rated wind speed).

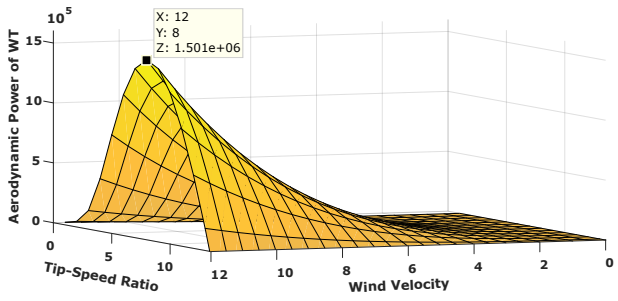

Fig. 5: Aerodynamic power of wind turbine .

3.2. DFIG-based Wind Turbine Dynamic Model

For dynamic modeling of DFIG-based wind turbines, a very useful and widely utilized model is used, it is called the Park's model or the Direct-Quadrature (dq) model [41]. It is assumed that the rotor and stator windings of the electrical generator model are placed symmetrically and sinusoidally, besides the effects of all the windings magnetic saturation are considered negligible. The stator and rotor generator dq frame is depicted in Fig. 6. The DFIG model can be described by the Eq. (4), Eq. (5), Eq. (6), Eq. (7) and Eq. (8):

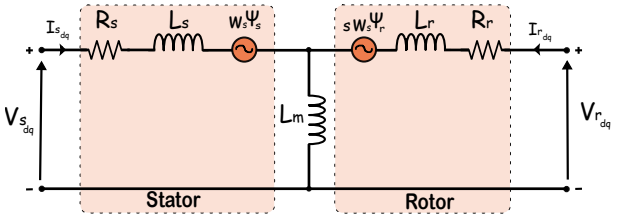

Fig. 6: Equivalent model diagram of the DFIG in dq.

$$\begin{bmatrix} v_{sd} \\ v_{sq} \end{bmatrix} = [R_s] \begin{bmatrix} i_{sd} \\ i_{sq} \end{bmatrix} + \frac{\mathrm{d}}{\mathrm{d}t} \begin{bmatrix} \Psi_{sd} \\ \Psi_{sq} \end{bmatrix} + [\omega_s] \begin{bmatrix} \Psi_{sd} \\ \Psi_{sq} \end{bmatrix}, \tag{4}$$

with: $[R_s] = \begin{bmatrix} R_s & 0 \\ 0 & R_s \end{bmatrix}$, and $[\omega_s] = \begin{bmatrix} 0 & -\omega_s \\ \omega_s & 0 \end{bmatrix}$,

$$\begin{bmatrix} v_{rd} \\ v_{rq} \end{bmatrix} = [R_r] \begin{bmatrix} i_{rd} \\ i_{rq} \end{bmatrix} + \frac{\mathrm{d}}{\mathrm{d}t} \begin{bmatrix} \Psi_{rd} \\ \Psi_{rq} \end{bmatrix} + [\omega_r] \begin{bmatrix} \Psi_{rd} \\ \Psi_{rq} \end{bmatrix}, \tag{5}$$

with: $[R_r] = \begin{bmatrix} R_r & 0 \\ 0 & R_r \end{bmatrix}$, and $[\omega_r] = \begin{bmatrix} 0 & -s\omega_s \\ s\omega_s & 0 \end{bmatrix}$,

where Ψ i and v are the field linkage, the current and the voltage, respectively. L_s, R_s and L_r, R_r are the inductance and the resistance of the stator and rotor respectively; and ω_s is the electrical angular speed.
The expressions of the magnetic fields of the stator and rotor are given as follows:

$$\begin{bmatrix} \Psi_{sd} \\ \Psi_{sq} \\ \Psi_{rd} \\ \Psi_{rq} \end{bmatrix} = \begin{bmatrix} -L_s & 0 & L_m & 0 \\ 0 & -L_s & 0 & L_m \\ L_m & 0 & -L_r & 0 \\ 0 & L_m & 0 & -L_r \end{bmatrix} \begin{bmatrix} i_{sd} \\ i_{sq} \\ i_{rd} \\ i_{rq} \end{bmatrix}, \tag{6}$$

where: $L_s = L_m + L_{s\sigma}$ and $L_r = L_m + L_{r\sigma}$; with $L_{s\sigma}$, $L_{r\sigma}$ and L_m are the stator leakage; the rotor leakage and the mutual inductances, respectively.
The expression of the stator reactive and active powers (P_s, Q_s) and of the generator rotor (P_r, Q_r) can be expressed as:

$$\begin{bmatrix} P_s \\ Q_s \end{bmatrix} = \frac{3}{2} \begin{bmatrix} v_{sd} & v_{sq} \\ v_{sq} & -v_{sd} \end{bmatrix} \begin{bmatrix} i_{sd} \\ i_{sq} \end{bmatrix}, \tag{7}$$

$$\begin{bmatrix} P_r \\ Q_r \end{bmatrix} = \frac{3}{2} \begin{bmatrix} v_{rd} & v_{rq} \\ v_{rq} & -v_{rd} \end{bmatrix} \begin{bmatrix} i_{rd} \\ i_{rq} \end{bmatrix}. \tag{8}$$

3.3. Grid side Converter, Transformer and Cable Dynamic Models

As reported in [16], the models schemes of the cable, the transformer, and the filter are illustrated in Fig. 7. The mathematical models of these equipment's in the direct-quadrature frame are represented below.

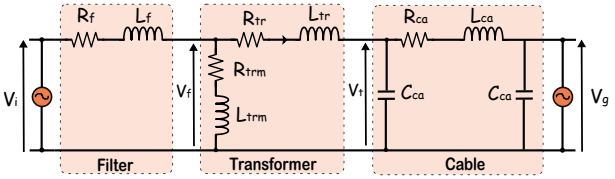

Fig. 7: Scheme simplified model of the cable, the transformer and the filter.

1) Grid Side Converter Model

To enhance power quality of wind turbine generators, we have included an RL filter between the power electronic converters and the power grid at the rotor side. The model of the filter-side can be described as:

$$\begin{bmatrix} v_{fd} \\ v_{fq} \end{bmatrix} = [L_f] \frac{\mathrm{d}}{\mathrm{d}t} \begin{bmatrix} i_{fd} \\ i_{fq} \end{bmatrix} + [A_f] \begin{bmatrix} i_{fd} \\ i_{fq} \end{bmatrix} + \begin{bmatrix} v_{id} \\ v_{iq} \end{bmatrix}, \quad (9)$$

with:

$$[L_f] = \begin{bmatrix} -L_f & 0 \\ 0 & -L_f \end{bmatrix},$$

$$[A_f] = \begin{bmatrix} -R_f & \omega_e L_f \\ -\omega_e L_f & -R_f \end{bmatrix},$$

where v_{fd} and v_{fq} represent the filter output voltages; i_{fd} and i_{fq} represent the filter currents; v_{id} and v_{iq} are the inverter output voltages; L_f and R_f represents the filter inductance and resistance. the exchanged powers (P_g, Q_g) with the power network are given by the following equations:

$$\begin{bmatrix} P_g \\ Q_g \end{bmatrix} = \frac{3}{2} \begin{bmatrix} v_{fd} & v_{fq} \\ v_{fq} & -v_{fd} \end{bmatrix} \begin{bmatrix} i_{fd} \\ i_{fq} \end{bmatrix}. \quad (10)$$

4. Mathematical Modeling of the ADRC Method

4.1. ADRC Structure

The majority of real systems are not only nonlinear and variable in time, but in addition, they are uncertain by presenting variations in the parameters described in their mathematical models. ADRC's control approach is a reliable control method developed by scientist Jingqing Han to address the limitations of the traditional PID approach [42]. To explain the concept of the ADRC approach, let us investigate a nonlinear controlled object with a single input and output, varying over time [43]:

$$\begin{cases} x(t)^n = f\left(x^{(n-1)}, x^{(n-2)}, \cdots, x, d, t\right) + b.u(t), \\ x(t) = y(t), \end{cases} \quad (11)$$

where: $z, \dot{z}, \ldots, z^n$ are respectively the state of the object and its different order dynamics, w corresponds to the external perturbations, $f\left(z^{(n-1)}, z^{(n-2)}, \cdots, z, d, t\right)$ denotes all relevant internal and external (total) perturbations impacting the controlled process, u and y are respectively the input and output of the process, respectively, and b is a process controlling coefficient.

In general, the dynamic model of the overall process and the controlling coefficients are usually hard to be established and to identified precisely. Numerous uncertainties exist; as a result, model-based control approaches and techniques have faced major challenges and complexities in the field of engineering applications [42]. The main strength of the ADRC lies in the fact that no matter how unclear and uncertain the dynamic model of the process is, and how many uncertainties the controlling coefficients presents, satisfactory control performances could be achieved. The fundamental design of the ADRC regulator is illustrated by the schematic layout in Fig. 8. It comprises three main parts: the TD (Tracking Differentiator), the ESO (Extended State Observer) and the NLSEF (Non Linear State Error Feedback) control law. Each of these three parts can take a variety of designs. For instance, if they include a non-linear link, it is named non-linear ADRC; on the contrary, if they are conceived as linear links, they are named linear ADRC [42]. The concepts of the three parts are outlined below.

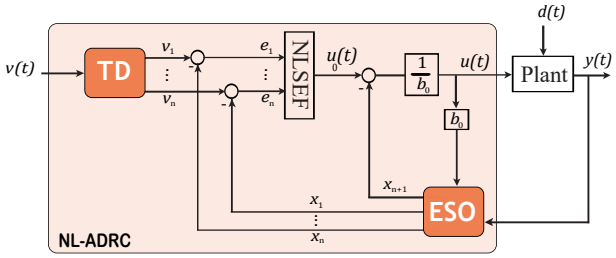

Fig. 8: Bloc diagram of nonlinear-ADRC structure.

In Fig. 8, v_i is the TD output signal which presents the tracking signals of the input signal v; x_i are the estimated signals; b_0 is the compensation factor; u_0 is the NLSEF given initial control amount; u is the given final control amount after perturbation cancellation.

1) Tracking Differentiator TD

The main objective of the tracking differentiator is to set up the transition of a given signal according to the controlled object input limits. While obtaining a smooth input, it also provides the differential signal of each order of this input. For n-th order uncertain systems, an n-th order tracking differentiator is usually used, and its standard form is given in [44].

2) Extended State Observer ESO

The ESO is the main component of the entire approach. It not only undertakes the task of estimating the state variables of the system and their differential signals of various orders, but also accurately comprehends the overall disturbances caused by changes in the internal parameters of the system and the external environment.

At this point, it is supposed that the entire process dynamic model is totally unknown, and the "overall perturbation" $f(\cdot)$, is approximated in real-time by the extended state.

Supposing that $z_1{=}z, \cdots, z_n = z^{n-1}$, let $z_{n+1} = f(\cdot)$ be the exteneded state variables of the process, the design of an ESO-NL is detailed in [45].

According to some circumstances, the ESO can approximate the state of the object and the overall perturbation of the process with some precision, which is:

$$x_1 \to z_1, \cdots, x_n \to z_n, \;\; x_{n+1} \to f(\cdot). \tag{12}$$

For the custom conception of the ESO, a variety of available observation and filter methods may be employed for the particular design of the ESO. The researcher Jingqing Han has selected $g_i(e)$ as the typical function, having the following formula [45]:

$$g_i(e) = fal(e, a_i, \delta) = \begin{cases} |e|^{a_i} sgn(\varepsilon) & |e| > \delta, \\ \dfrac{e}{\delta^{1-a_i}} & |e| \leq \delta, \end{cases} \tag{13}$$

where: $0 < a_i < 1$, and $\delta > 0$ are configurable factors; if $a_i = 1$, $g_i(e) = e$. The obtained result is a traditional Luenberger observer, so-called the Linear ESO.

3) State Error Feedback Control Law

The ESO acquires in real time the predicted amount of the overall perturbation. If this amount is cancelled out in the control law, the function of perturbations rejection is then achieved. Consequently, the control law is considered to be as follows [46]:

$$u = \frac{u_0 - x_{n+1}}{b_0}, \tag{14}$$

where u_0 is the initial amount of control. If the prediction error of x_{n+1} on the overall perturbation "$f(\cdot) + (b{-}b_0)u$" is removed, the process (11) is transformed to a "series of integrators":

$$z^n = f(\cdot) + (b{-}b_0)u - x_{n+1} + u_0 \approx u_0. \tag{15}$$

In this manner, the process which contains a large quantity of perturbations, uncertainties and nonlinearities is consistently transformed into a typical types of integrators, rendering the conception of the control scheme from complicated to simple and has a wide applicability.

The control amount u_0 has several applications [47], the expression of a general Non Linear State Error Feedback (NLSEF) control for any order controlled process is given in [45]. To reduce the model complexity and design compared to the nonlinear ADRC, in this paper the Linear ADRC is adopted and utilized to ensure the extraction of the maximum wind power as well as to control the wind turbine converters.

4.2. Linear ADRC Structure

As indicated in the previous part, the ADRC control technology can be divided to linear and nonlinear strategies, owing to the usage of nonlinear functions in all three elements of the ADRC, and taking into account the difficulties in practical applications, we have used and developed in this paper a linear-ADRC control technology, which is proposed in [48], the ADRC controller parameters are tuned based on the bandwidth.

As mentioned in the previous section, the control technology of ADRC can be divided into linear and nonlinear strategies, due to the use of nonlinear functions in the three elements of ADRC, and considering the difficulties in practical applications, in this work, we used and developed a linear-ADRC control technology, which is proposed in [48], the parameters of the ADRC controller are tuned based on the bandwidth. The basic idea of bandwidth is a performance index of the response control process. The faster it is, the better the immunity. Therefore, when designing the controller and the extended state observer, the bandwidth can be used as the only tunable parameter of the system, and the remaining parameters are converted into functions of the bandwidth.
To illustrate the principle of the linear ADRC [46], the system in Eq. (11) is considered and rewritten in the following form (Known as the ADRC canonical form):

$$y^{(n)} = f(\cdot) + b_0 \cdot u. \tag{16}$$

Assuming $f(\cdot)$ is differentiable while taking $\dot{f}(\cdot) = h$. The Eq. (16) could be written as follows:

$$\begin{cases} \dot{x} = \mathbf{A}z + \vec{B}u + \vec{G}h, \\ y = \vec{C}x, \end{cases} \tag{17}$$

where :

$$\vec{x} = [x_1 \quad x_2 \quad \cdots \quad x_n \quad x_{n+1}]^T,$$

$$\mathbf{A}_{(n+1,n+1)} = \begin{bmatrix} 0 & 1 & 0 & \cdots & 0 \\ 0 & 0 & 1 & \cdots & 0 \\ \vdots & \vdots & \vdots & \ddots & \vdots \\ 0 & 0 & 0 & \cdots & 1 \\ 0 & 0 & 0 & \cdots & 0 \end{bmatrix},$$

$$\vec{B}_{(n+1,1)} = [1 \quad 0 \quad \cdots \quad b_0 \quad 0]^T,$$

$$\vec{C}_{(n+1,1)} = [1 \quad 0 \quad \cdots \quad 0 \quad 0],$$

$$\vec{G}_{(n+1,1)} = [0 \quad 0 \quad \cdots \quad 0 \quad 1]^T.$$

As a result, the ESO can be designed as a full-order Luenberger observer which is given as follows:

$$\begin{cases} \dot{\hat{x}} = \mathbf{A}\hat{x} + \vec{B}u + \vec{L}(y - \hat{y}), \\ \hat{y} = \vec{C}\hat{x}, \end{cases} \tag{18}$$

where the vector $\vec{L}$ represents the observer gains.

The error obtained by the observer is given by:

$$e = x - \hat{x}, \tag{19}$$

its dynamics is then written as:

$$\dot{e} = (\mathbf{A} - \mathbf{LC})\, e, \tag{20}$$

With:

$$\mathbf{A} - \mathbf{LC} = \begin{bmatrix} -\beta_{01} & 1 & 0 & \cdots & 0 \\ -\beta_{02} & 0 & 1 & \cdots & 0 \\ \vdots & \vdots & \vdots & \ddots & \vdots \\ -\beta_{0n} & 0 & 0 & \cdots & 1 \\ -\beta_{0(n+1)} & 0 & 0 & \cdots & 0 \end{bmatrix}.$$

To obtain a good functioning of the observer ($e \to 0$ when $t \to \infty$) , the $\mathbf{L}$ matrix gains should be chosen in the way that $(\mathbf{A} - \mathbf{LC})$ constitutes a Hurwitz matrix, which means that its polynomial characteristic poles of $P_{ESO}(s)$ all have strictly negative parts [49].

$$P_{ESO}(s) = \det\left(sI_{n+1} - (\mathbf{A} - \mathbf{LC})\right), \tag{21}$$

Then:

$$P_{ESO}(s) = s^{n+1} + \beta_1 s^n + \cdots + \beta_n s + \beta_{(n+1)}. \tag{22}$$

Generally, the pole placement technique is used to determine the observer's gains. A balance must be struck between the observer tracking speed and its noise measurement sensitivity. As the ESO becomes faster, the perturbation is anticipated early and then removed by the controller. It is done by positioning the poles of the observer just to the left of the controlled process in the *P-plan*. This results in the implementation of a significant bandwidth for ESO. Nevertheless, it must be mentioned that as the bandwidth increases, the system can be damaged by allowing the propagation of noise [49].

By considering all these conditions, the cut-off pulse of the ESO ω_o is then selected in such that it has an appropriate settling time. As a result, the $(n+1)$ poles are positioned at $-\omega_o$.

$$P_{ESO}(s) = (s + \omega_o)^{n+1}. \tag{23}$$

The expression of the observer's coefficients is then given as follows:

$$\beta_{0i} = \frac{(n+1)!}{(n+1-i)!i!}\omega_o^i. \tag{24}$$

As a result, when $\mathbf{A} - \mathbf{LC}$ is stable, $\hat{x}_1, \hat{x}_2, \ldots, \hat{x}_n$ will approach y and its derivatives, and $\hat{z}_{n+1}$ will approach the overall perturbation $f(\cdot)$. Consequently, the final control amount can take into condideration those estimated disturbances and reject them in real time.

If the final control law amount is taken as:

$$u = \frac{u_0 - \hat{x}_{n+1}}{b_0}, \tag{25}$$

then the system in Eq. (16) becomes:

$$y^{(n)} = f(\cdot) - \hat{x}_{n+1} + u_0. \tag{26}$$

If $\hat{x}_{n+1}$ is a good estimation of $f(\cdot)$ ($\hat{z}_{n+1} \approx f(\cdot)$), an integral process of $n-$order is obtained.

$$y^{(n)} = u_0. \tag{27}$$

Which could be then controlled by the control law given as:

$$u_0 = k_1(r - y) + k_2(\dot{r} - \dot{y}) + \cdots + k_n(r^{(n+1)} - y^{(n+1)}), \tag{28}$$

where: r represents the reference signal.

As $\hat{x}_1, \ldots, \hat{x}_n$ is a a good approximation of $y, \ldots, y^{(n-1)}$, the overall control amount is then expressed as:

$$u = K_p(\hat{r} - \hat{x}) \tag{29}$$

where:

$$\hat{r} = \begin{bmatrix} r & \dot{r} & \ldots & r^{(n-1)} & 0 \end{bmatrix}^T,$$

and

$$K_p = \frac{[k_1 \quad k_2 \quad \ldots \quad k_n \quad 1]}{b_0},$$

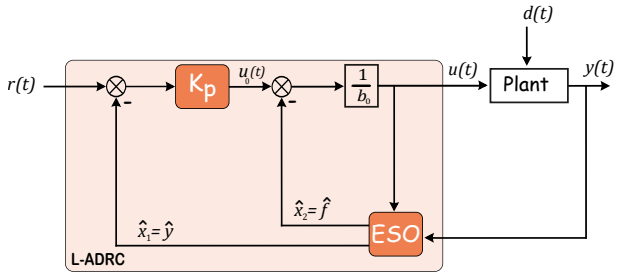

Fig. 9: Block of a linear-ADRC controller structure [8].

The Linear ADRC can be then summarized and designed as follows:

$$\begin{cases} \dot{\hat{x}} = (A - LC)\hat{x} + Bu + Ly, \\ u = K_0[\hat{r} - \hat{x}]. \end{cases} \tag{30}$$

In summary, the structure of a first order linear-ADRC approach is displays in Fig. 9

5. ADRC Control Strategy of a DFIG-Based Wind Turbine

This section deals with the proposed control strategy of the wind turbine; its objectives are the control active power and reactive power of WTs at Point of Common Coupling (PCC). Moreover, the active power control can be used to regulate the powers generated by DFIG either in its stator and rotor. On the other hand, the reactive power control is used to regulate the total reactive power capability of stator and grid side. To overcome the problem of disturbances we have integrated the active disturbance rejection control method, as we have shown in the previous section, the non-linear ADRC is a complicated control method and has various parameters needed to be tuned which cause difficulties in practical applications. Therefore, a Linear ADRC approach is then given and applied to the DFIG-based WT.

Figure 10 displays the global scheme of a wind turbine system controlled by the ADRC Strategy, we have divided the control system into two parts: rotor-side control and grid-side control.

5.1. Control by ADRC of the Rotor-Side Converter

The rotor-side converter control strategy is designed to independently control the active power and reactive power of the DFIG stator. To ensure this aim, the Indirect Stator Field Oriented Technical (ISFOT) is then applied; where the stator field vector Ψ_s is aligned to the d axis. Thereafter, the components of the stator fields are $\Psi_{sd} = \Psi_s$; $\Psi_{sq} = 0$. Besides this for high-powered generators used in wind power systems, a negligible stator resistance R_s is assumed.
Therefore, the DFIG model Eq. (5) becomes Eq. (31) and can be written as:

$$\frac{\mathrm{d}}{\mathrm{d}t}\begin{bmatrix} i_{rd} \\ i_{rq} \end{bmatrix} = [L_1]\begin{bmatrix} i_{rd} \\ i_{rq} \end{bmatrix} + \begin{bmatrix} -\omega_r k_3 \Psi_s \\ 0 \end{bmatrix} + [L_2]\begin{bmatrix} v_{rd} \\ v_{rq} \end{bmatrix}, \tag{31}$$

with: $[L_1] = \begin{bmatrix} -k_1 & s\omega_g \\ -s\omega_g & -k_1 \end{bmatrix}$, $[L_2] = \begin{bmatrix} k_2 & 0 \\ 0 & k_2 \end{bmatrix}$,

where:
$k_1 = \frac{R_r}{\sigma L_r}$; $k_2 = \frac{1}{\sigma L_r}$; $k_3 = \frac{Lm}{\sigma L_s L_r}$; $\omega_r = \omega_g - p\Omega_{mec}$.

The expressions of the stator powers can be expressed as follows:

$$P_{s_i} = -\frac{3}{2}\frac{L_m}{L_s}\, v_g i_{rq}, \tag{32}$$

$$Q_{s_i} = \frac{3}{2}(-\frac{L_m}{L_s}\, v_g i_{rd} + \frac{\Psi_s}{L_s} v_g). \tag{33}$$

The reference currents i_{rq}^{ref} and i_{rq}^{ref} are calculated by the desired delivery of of WTs:

$$i_{rq}^{ref} = -\frac{2}{3}\frac{L_s}{v_g\, L_m}\, P_{s\_i}^{ref}, \tag{34}$$

$$i_{rd}^{ref} = \frac{\Psi_s}{L_m} - \frac{2}{3}\frac{L_s}{v_g L_m} Q_{s\_i}^{ref}, \tag{35}$$

where $P_{s\_i}^{ref}$ and $Q_{s\_i}^{ref}$ are the power references of stator side which are imposed by the local supervisory unit of the wind generator i^{th} .
For the conception of the rotor side Linear-ADRC controller, the regulations of the rotor currents are achieved by adoption of two ADRC regulators as shown in Fig. 10, wherein the equations Eq. (31) are adapted to the canonical form of Linear-ARDC as follows:

$$\dot{y}(t) = f(t) + b_0\, u(t). \tag{36}$$

Therefore, the d-axis rotor current i_{rd} control loop design by Linear-ADRC is:

$$\begin{cases} f_{i_{rd}} = -k_1\, i_{rd} + s\omega_g\, i_{rq} + (k_2 - b_0^{i_{rq}})\, v_{rq}, \\ b_0^{i_{rd}} = k_2, \\ u_{i_{rd}} = v_{rd}. \end{cases} \tag{37}$$

And the q-axis rotor current i_{rq} control loop design by Linear-ADRC is:

$$\begin{cases} f_{i_{rq}} = -k_1 i_{rq} + \omega_r i_{rd} - \omega_r k_3 \Psi_s + (k_2 - b_0^{i_{rq}}) v_{rq}, \\ b_0^{i_{rq}} = k_2, \\ u_{i_{rq}} = v_{rq}. \end{cases} \tag{38}$$

where: $f_{i_{rd}}$ and $f_{i_{rq}}$ are the generalized disturbance; $u_{i_{rd}}$ and $u_{i_{rq}}$ are the control amounts.

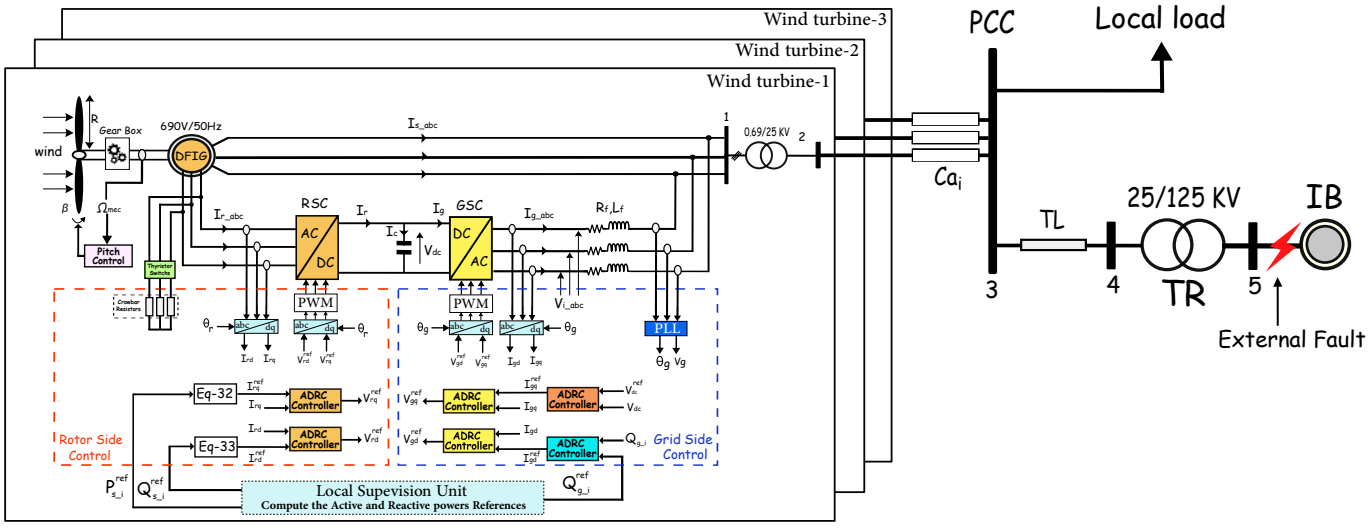

Fig. 10: Global scheme of a DFIG-based wind turbine using a ADRC strategy control

5.2. Control by ADRC of the Grid-Side Converter

The GSC control is utilized for the regulation of the injected power to the electrical power network by the control of the DC-bus voltage, and the regulation of the grid side reactive power according to the demand. In terms of rotor-side, we used the Voltage Oriented Technique (VOT), where the network voltage is oriented along the d axis as follows: $v_{gd} = 0$; $v_{gq} = v_g$.

- Design of Grid Currents Controller:

The line grid-side converter model Eq. (9) becomes Eq. (39) and can be written as:

$$\frac{\mathrm{d}}{\mathrm{d}t}\begin{bmatrix} i_{fd} \\ i_{fq} \end{bmatrix} = [L_3]\begin{bmatrix} i_{fd} \\ i_{fq} \end{bmatrix} + [L_4]\begin{bmatrix} v_{id} \\ v_{iq} \end{bmatrix} + \begin{bmatrix} 0 \\ -k_5 v_g \end{bmatrix}, \quad (39)$$

with: $[L_3] = \begin{bmatrix} -k_4 & \omega_g \\ -\omega_g & -k_4 \end{bmatrix}$, $[L_4] = \begin{bmatrix} k_5 & 0 \\ 0 & k_5 \end{bmatrix}$,

where: $k_4 = \frac{R_f}{L_f}$; $k_5 = \frac{1}{L_f}$.

The Linear-ADRC controllers for the currents of the GSC are designed as follows:

For linear-ADRC controller for d-axis grid-side current loop i_{fd}:

$$\begin{cases} f_{i_{fd}} = -k_4\ i_{fd} + \omega_g\ i_{fq} + (k_5 - b_0^{i_{fd}})\ v_{id}, \\ b_0^{i_{fd}} = -k_5, \\ u_{i_{fd}} = v_{id}. \end{cases} \quad (40)$$

And linear-ADRC controller for q-axis grid-side current loop i_{fq}:

$$\begin{cases} f_{i_{fq}} = -k_4\ i_{fq} + \omega_g\ i_{dq} + (k_5 - b_0^{i_{fq}})\ v_{iq}, \\ b_0^{i_{fq}} = -k_5, \\ u_{i_{fq}} = v_{iq}. \end{cases} \quad (41)$$

where: $f_{i_{fd}}$ and $f_{i_{fq}}$ are the generalized disturbance affecting the grid-side currents i_{fd} and i_{fq} respectively; $u_{i_{fd}}$ and $u_{i_{fq}}$ are the control amounts.

- Design of DC-link voltage Controller:

In order to design the Linear-ADRC controller of the DC-link voltage control, and motivated by the works in [50] and [51] all the losses in converters are supposed neglected, thus P_r and P_f are given by those expressions $P_r = i_r v_{dc}$ and $P_f = i_f v_{dc}$.
Hence, the DC-Bus voltage expression becomes as:

$$\frac{\mathrm{d}v_{dc}^2}{\mathrm{d}t} = \frac{2}{C}P_r - \frac{3}{C}v_g i_{fq}. \quad (42)$$

We put $U = {v_{dc}}^2$, therefrom the DC-Link voltage equation becomes as:

$$\frac{\mathrm{d}U}{\mathrm{d}t} = k_6 P_r - k_7 i_{fq}, \quad (43)$$

with $k_6 = \frac{2}{C}$; $k_7 = \frac{3}{C}v_g$.

After adaption of the DC-Bus voltage expression to the ADRC form, the Linear-ADRC controller is then obtained and it is designed as follows:

$$\begin{cases} f_{v_{dc}} = -k_6 P_r + (-k_7 - b_0^{v_{dc}}) i_{fq}, \\ b_0^{v_{dc}} = k_7, \\ u_{v_{dc}} = i_{fq}. \end{cases} \quad (44)$$

- Design of Grid Reactive Power Controller:

To achieve an effective regulation of the reactive power problem at the PCC, it is necessary to control the reactive power of each wind generator, which can be achieved by using the ADRC controller. As a result,

to design the ADRC regulator of reactive power control, we have established for the control loops, the transformer and the transmission cable dynamic model [16]. The regulation of the grid reactive power is then achieved by adoption of a Linear-ADRC controller, wherein its canonical form is given by:

$$\dot{y}(t) = f(y, d, u) + b_0 u(t), \tag{45}$$

with $f(y, d, u)$ represents the total (internal and external) disturbance, b_0 is known part of the process (system), $d(t)$ represents the external disturbance and $u(t)$, $y(t)$ are input and output of the process respectively.

As in [16] and [52], the expression of the exchanged reactive power exchange with the grid can be given by:

$$\frac{\mathrm{d}Q_g}{\mathrm{d}t} = -k_8\ i_{fd} - k_8\ \omega_g\ i_{fq} - v_{fd}, \tag{46}$$

where: $k_8 = \frac{3}{2}\frac{R}{L} v_g$, and the resistance $R{=}R_{tr}{+}R_{ca}$, the inductance $L{=}L_{tr}{+}L_{ca}$.

Therefore, the design of the Linear-ADRC for reactive power control, after adaption of the exchange reactive power with the grid equation to the ADRC canonical form as follows:

$$\begin{cases} f_{Q_g} = -k_8\ \omega_g\ i_{fq} - v_{fd} + (-k_8 - b_0^{Q_g})\ i_{fd}, \\ b_0^{Q_g} = k_8, \\ u_{Q_g} = i_{fd}, \end{cases} \tag{47}$$

where: f_{Q_g} is the total (external and internal) disturbances affecting the reactive power, $b_0^{Q_g}$ is the known parts of the system parameters.

6. Supervisory Control of a DFIG-Based Wind Farm

6.1. Proposed PD Algorithm for the DFIG Based Wind Farm

The supervisory control on the basis of the proportional distribution algorithm was designed in order to dispatch the power proportionally on the wind generators. In terms of security, this algorithm guarantees that the individual wind generators will always be operating for beyond their boundaries as determined by the plan ($Q_{wg\_i}^{\max}$, $Q_{wg\_i}^{\max}$) [50]. However, the advantage of this strategy is that it ensures that all of the wind turbines of the farms operate sufficiently away from their maximum generation capacity so that there is no risk of saturation of the wind turbines. This approach provides the active and reactive power references of each wind turbine $P_{wg\_i}^{ref}$ and $Q_{wg\_i}^{ref}$ from the references of the total powers demanded by the grid operator P_{wf}^{ref} and Q_{wf}^{ref}. Therefore, the expressions of a wind generator active and reactive powers references are as follows:

$$P_{wg\_i}^{ref} = \frac{P_{wg\_i}^{\max}}{P_{wf}^{\max}} P_{wf}^{ref}, \tag{48}$$

$$Q_{wg\_i}^{ref} = \frac{Q_{wg\_i}^{\max}}{Q_{wf}^{\max}} Q_{wf}^{ref}, \tag{49}$$

where $P_{wf}^{\max}$ and $Q_{wf}^{\max}$ are the maximum active and reactive powers of wind farm.

The farm maximum power capacity can be approximated by using the summation of all the individuals wind generators available maximum active and reactive powers:

$$P_{wf}^{\max} = \sum_{j=1}^{n} P_{wg\_i}^{\max}, \tag{50}$$

$$Q_{wf}^{\max} = \sum_{j=1}^{n} Q_{wg\_i}^{\max}, \tag{51}$$

where $P_{wg\_i}^{\max}$ and $Q_{wg\_i}^{\max}$ are the maximum active and reactive powers of the wind turbine i^{th} respectively, n is the number of the farm WGs.

Wherein, the maximum active power available from the wind generator i^{th} is given by Eq. (52), and the maximum reactive power that can be exchanged by the line-side converter of each WGs and the grid can be expressed using Eq. (53):

$$P_{wg\_i}^{\max} = P_{opt\_i}, \tag{52}$$

$$Q_{wg\_i}^{\max} = Q_{s\_i}^{\max} + Q_{g\_i}^{\max}, \tag{53}$$

where $Q_{s\_i}^{\max}$ and $Q_{g\_i}^{\max}$ are the maximum reactive power of stator of DFIG and grid side for wind generator i^{th} respectively.

6.2. Centralized Supervisory Unit of DFIG-Based Wind Farm

To overcome the stability concern problems of the electrical power system and its power quality and reliability, the transmission system operator must manage the WF as a conventional power plant. Thanks to the local supervisory unit and the central supervisory unit, the wind farm is installed in the purpose of controlling the powers (P_{wf}, Q_{wf}) exchanged with the power grid, taking into account to the current state of the power grid and the control mode demanded by the grid operator (MPPT, balance, delta, fault,..., etc.) control. The supervisory and management power system configuration of the WF based on DFIG generator is depicted in Fig. 11.

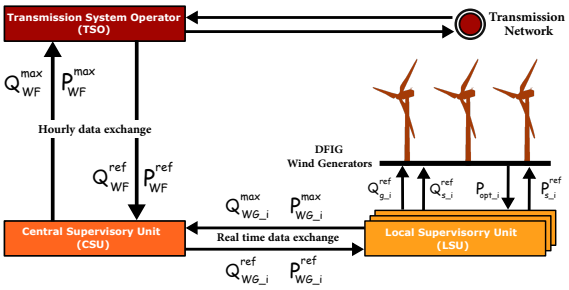

Fig. 11: Supervisory power system configuration.

6.3. Central Supervisory Unit of WF

The CSU is one of the most important elements of the power wind farms, whose main purpose is to monitor the total powers of the WF and to comply with the generation plan requested every hour by the system operator (P_{wf}^{ref}, Q_{wf}^{ref}).

The CSU obtains the desired quantity of power requested by the TSO and sends the power generation capacity information ($P_{wf}^{\max}$, $Q_{wf}^{\max}$) to the TSO. By implementing the PD algorithm, the proportional power references for each wind generator on the farm ($P_{wg\_i}^{ref}$, $Q_{wg\_i}^{ref}$) are calculated according to the above equations and will be delivered to the local supervisory units in real-time.

6.4. Local Supervision Unit of WTs

To manage the power dispatch between the stator ($P_{s\_i}^{ref}$, $Q_{s\_i}^{ref}$) and the grid sides ($P_{g\_i}^{ref}$, $Q_{g\_i}^{ref}$) toward producing the reference of active power $P_{wg\_i}^{ref}$ and the reference of reactive power $Q_{wg\_i}^{ref}$ of wind generator i^{th}, this coordination ensured by the local supervisory unit which incorporated inside each wind turbine. Meanwhile, it estimates in real time the maximum powers ($P_{wg\_i}^{\max}$, $Q_{wg\_i}^{\max}$) that can produce each wind generator and send them to the CSU.

Local management algorithm of the active and reactive power dispatching using to control the wind turbines depending on one of the management modes (MPPT mode, Fault mode or PQ mode) which are developed hereafter.

1) Optimal Power Control (or MPPT) Mode

The optimal power control (MPPT control) of the system is used to capture the maximum available power from the wind turbines, it is necessary to adjust the generator mechanical speed by acting on the electromagnetic torque in order to maintain the TSR to its optimum value ($\lambda = \lambda^{opt}$) and the power coefficient ($C_p = C_p^{\max}$) for a given value of the blades pitch angle $\beta = 0°$ [53].

Therefore, the optimal aerodynamic power (maximum power) is then given by the following equation:

$$P_{opt\_i} = \frac{1}{2}\,\rho\,\pi\,R^5\,\frac{C_p^{\max}}{\lambda^{opt^3}}\,\frac{1}{p^3\,G^3}\,\omega_{mec\_i}^3, \tag{54}$$

where R and ρ are representing the turbine radius blades and the air density respectively. ω_{mec_i} is the mechanical angular speed of the WT i^{th}.
The reference of the stator power in this mode is such that:

$$P_{wf\_i}^{ref} = P_{opt\_i} = K_{opt}\,\omega_{mec\_i}^3, \tag{55}$$

where the optimal power coefficient K_{opt} is :

$$K_{opt} = \frac{1}{2}\,\rho\,\pi\,R^5\,\frac{C_p^{\max}}{\lambda^{opt^3}}\,\frac{1}{p^3\,G^3}. \tag{56}$$

In this mode, the GSC takes into account all the reactive power needed and the stator of the DFIG is utilized to generate only the maximum active power [50]. In our case, we will have a unity power factor at PCC. Hence, the expressions of the reactive powers references are:

$$\begin{cases} Q_{s\_i}^{ref} = 0, \\ Q_{g\_i}^{ref} = 0. \end{cases} \tag{57}$$

2) Fault Control Mode

The fault mode is implemented and activated once a voltage failure is detected. Whenever the voltage drop of the grid occurs $0.9 \geq V_{pcc_{pu}}$, the behavior of the wind power system becomes unstable and it is unable to generate both reactive and active powers. Nevertheless, using the suggested control method on the wind power system for controlling the active and reactive power of the WTs to withstand the voltage fault, and also crowbar shorting resistors on the DFIG rotor, to provide protection of the system from overcurrent and resulting overvoltage in the rotor circuit and in the DC link. As a result, the wind turbine system operates as a STATCOM and shall therefore provide the demanded reactive power up to its maximum boundaries. Further, according to the German GC depicted in Fig. 3(b), the reference of the reactive current to be supplied to the network according to the voltage amplitude during the fault can be calculated as follows [53]:

$$I_{gr}^{ref} = \begin{cases} k(1 - V_{g_{pu}})I_{gr_n} & \text{if } 0.9 \geq V_{pcc_{pu}} > 0.5, \\ I_{gr_n} & \text{if } V_{pcc_{pu}} \leq 0.5, \end{cases} \tag{58}$$

where I_{gr}^{ref} is the reference reactive grid current, I_{r_n} is the reactive current reference; $V_{g_{pu}}$ is the per unit value of the grid voltage during the perturbation

from its nominal value and k is a constant given equal to 2. Consequently, the expression of the supplied reactive power according to the grid voltage amplitude is determined as:

$$Q^{ref}_{frt\_i} = Q^{ref}_{wf} = \frac{3}{2} V_{pcc} I^{ref}_{gr}. \tag{59}$$

According to the quantity of reactive power demand ($Q^{ref}_{frt\_i}$), the reactive power expression of rotor side and grid side are calculated using the Eq. (60) and Eq. (61).

If the stator reactive capacity is sufficient to meet the reactive power requirements of the grid operator, the grid side converter must operate at unity power factor. Therefore, the DFIG stator is responsible for supplying or absorbing all of the reactive power demanded from the WT. In this case, the reactive power of the wind turbine verifies the following constraints:

$$\begin{cases} Q^{ref}_{s\_i} = Q^{ref}_{wg\_i}, \\ Q^{ref}_{g\_i} = 0. \end{cases} \tag{60}$$

On the other hand, if the demanded reactive power of the WT is higher than the stator maximum reactive capacity, the GSC contributes along with the stator to the generation or absorption of the corresponding reactive power. Thus, the expression of the reference reactive powers is as follows:

$$\begin{cases} Q^{ref}_{s\_i} = Q^{\max}_{s\_i}, \\ Q^{ref}_{g\_i} = Q^{ref}_{wg\_i} - Q^{\max}_{s\_i}. \end{cases} \tag{61}$$

As indicated in the introduction, if the DFIG-based wind generators cannot operate properly during the fault without any protection system, then we used the crowbar with series braking resistors. The optimal value of crowbar resistance R_{crw_opt} as indicated in [54] is given by the following equation:

$$R_{crw\_opt} = \frac{\sqrt{2}(V_{r\_\max}\omega_s L_s)}{\sqrt{(3.2V_s^2 - 2V^2_{r\_\max})}}. \tag{62}$$

3) PQ Control Mode

In some cases, the grid operator demands a specific quantity of active and reactive power. For this, the PQ mode is used to force the wind farm to provide an active power and provide and consume a reactive power given by the TSO. It guarantees to provide the maximum capacity or less of the active power generation, through rotor side converter control, and the management of reactive power exchange between a wind farm and network through two sides (rotor and grid).

The expression of a wind turbine's active and reactive powers references for this mode are given in equations Eq. (48) and Eq. (49). The stator reference active powers for the DFIG-based WTs ($P^{ref}_{s\_i}$) calculated from the reference active powers of the WTs $P^{ref}_{wg\_i}$ can given by following equations:

$$P^{ref}_{s\_i} = P^{ref}_{wg\_i} - P_{r\_i}. \tag{63}$$

In contrast, if the required reactive power is superior to the generated reactive power, the wind farm must compromise an amount of active power to satisfy the demand under some conditions, the first condition is that the reactive power reference imposed by the supervisory system does not exceed the maximum value given in Eq. (53), and the second is the expression of the active power reference obtained by utilizing ($Q^{ref}_{wg\_i}$) and the rated apparent power of i^{th} of the wind turbine ($S_{wg_{n\_i}}$):

$$P^{ref}_{wg\_i} = \sqrt{S^2_{wg_{n\_i}} - {Q^{ref}_{wg\_i}}^2}. \tag{64}$$

Finally, in order to set up the supervision algorithm of DFIG-based wind farm, the algorithm control must be followed as summarized and presented in Appendix 1.2.

7. Simulation Results and Discussion

To validate the analytical results of the proposed control strategies, the DFIG-based WF full model, and its supervisory control approaches illustrated in Fig. 4 and Fig. 11 were carried out in Matlab/Simulink environment, with the parameters of the simulation given in the table of Appendix 1.1. The wind farm consists of three DFIG wind turbines with a total capacity of 4.5 MW, applied types of wind profiles to each WT as shown in Fig. 14.

To study and validate the effectiveness of the active and reactive powers management by the proposed control strategy in this paper, the introduced simulation tests are divided into three intervals; each interval contains one of the controls modes (MPPT, PQ or voltage fault) controls.

7.1. Test 1: Supervisory System Control of the WF

In this performed test, the objective is to verify and validate the supervisory power management system and the dynamic behavior of the WF, according to a network operator plan while taking into account the adopted proportional distribution algorithm, the scenario is taken as:

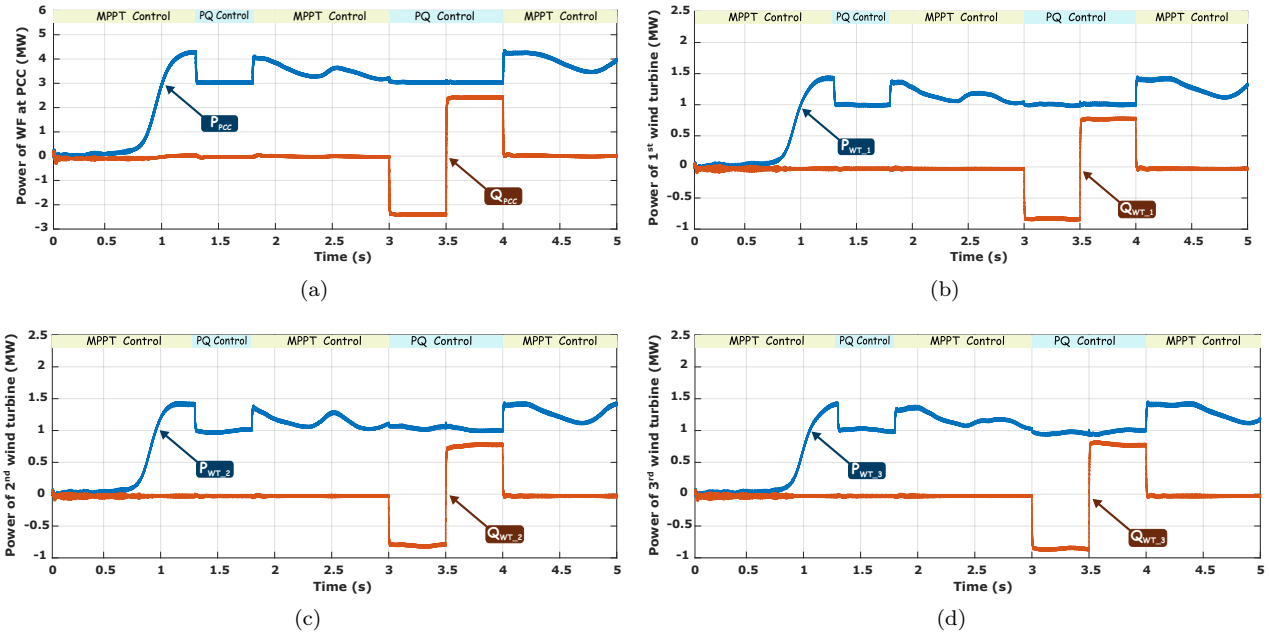

Fig. 12: Simulation results of test 1 (P_i,Q_i): (a) of the WF, (b) of the 1^{st} WT, (c) of the 2^{nd} WT, (d) of the 3^{rd} WT.

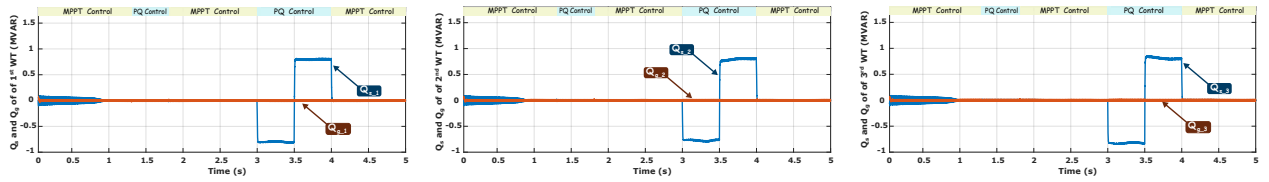

Fig. 13: Simulation results of test 1 (Q_{s_i},Q_{g_i}): (a) of the 1^{st} WT, (b) of the 2^{nd} WT, (c) of the 3^{rd} WT.

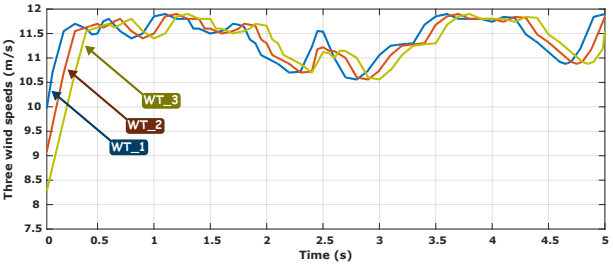

Fig. 14: Wind Speeds.

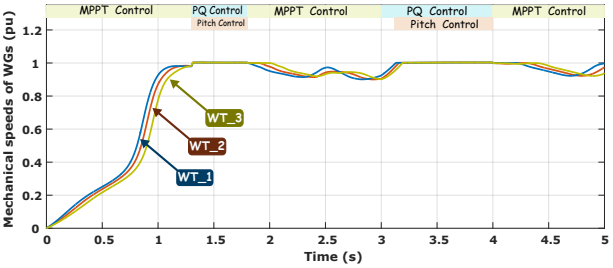

Fig. 15: Mechanical generators speed.

- Interval 1: the MPPT control is selected from 0 s to 1.3 s, to generate the maximum active power with the unity power factor ($Q_{pcc} = 0$ MVAR).
- Interval 2: the PQ control is activated from 1.3 s to 1.8 s. The demanded active power is set to 3 MW at PCC.
- Interval 3: the MPPT control is selected from 1.8 s to 3 s, to provide the maximum active power and a unit power factor at the rotor side and grid side.
- Interval 4: the PQ control is activated from 3 s to 4 s. Likewise, for interval 2, the required active power is equal to 3 MW, but for the reactive power from 3 s to 3.5 s, the WF consumes 2.4 MVAR and generates the same amount from 3.5 s to 4 s.
- Interval 5: the MPPT control is selected from 4 s to 5 s, to provide the maximum active power only.

As shown in Fig. 12, the wind farm responds to the demand of the grid operator to produce active power, and to the generate or consume reactive power during MPPT and PQ mode. These powers are distributed in a weighted way over the three wind turbines (Fig. 12(b), Fig. 12(c) and Fig. 12(d)) which shows the application of the PD algorithm for the centralized supervisory of the wind farm powers. The WF provides then the necessary reactive power while not exceeding

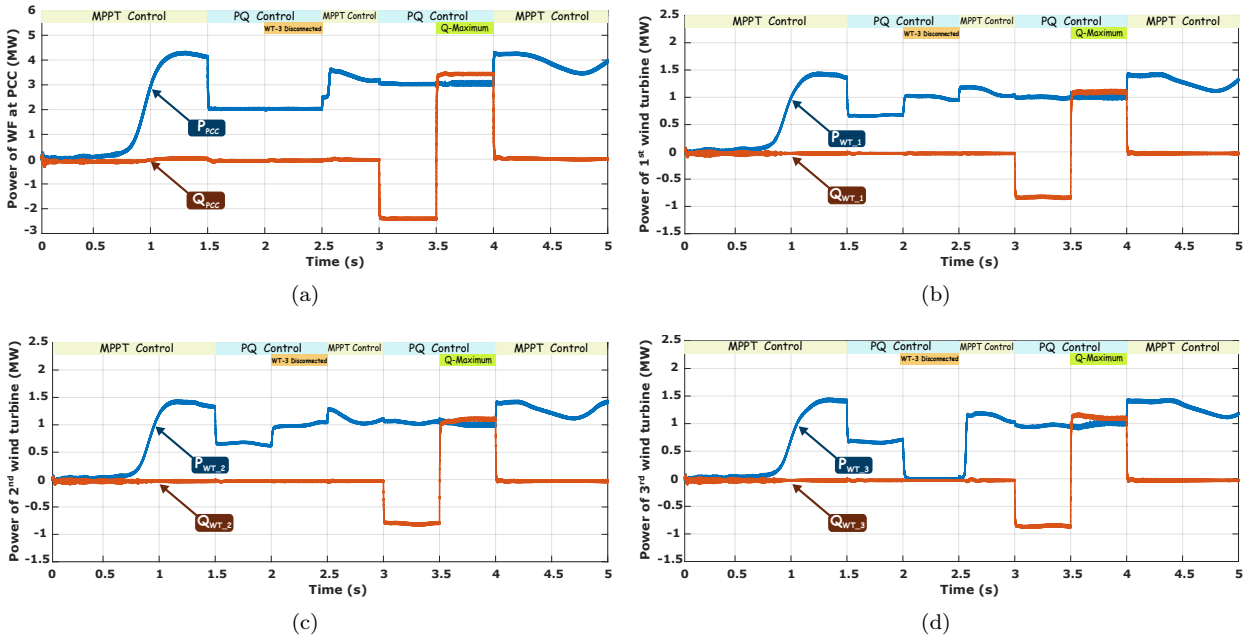

Fig. 16: Simulation results of test 2 (P_i, Q_i): (a) of the WF, (b) of the 1^{st} WT, (c) of the 2^{nd} WT, (d) of the 3^{rd} WT.

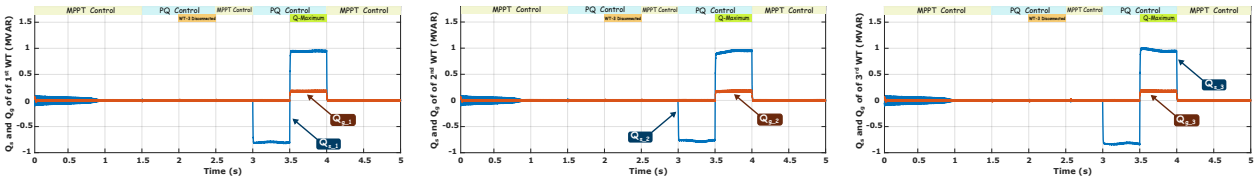

Fig. 17: Simulation results of test 2 (Q_{s_i},Q_{g_i}): (a) of the 1^{st} WF, (b) of the 2^{nd} WF, (c) of the 3^{rd} WF.

the limits of the three WTs. In this case, the reactive power supplied by the wind turbines is more than enough to satisfy the reactive power request of the WF. The GSCs are not required by the control system to assist to the reactive power generation and they operate at the unity power factor, as shown in Fig. 13.

Noteworthy, during PQ control (Intervals 2 and 4), the wind generators rotor speed is increased due to the decreases of the active power (electromagnetic torque) transmitted to the network, and by the pitch control, the mechanical speed of the wind generators does not exceed the rated value as illustrated in Fig. 15.

7.2. Test 2: Interactions Between the Wind Turbines

The purpose of this test to is investigate the dynamic behavior of the wind farm and the interaction among the wind turbines in which a disconnection of the third WT is occurred for a given duration. Moreover, to investigate the interaction of the WF in case of a highest demand of reactive power by the TSO, the scenario is as follows:

- Interval 1 [from 0 s to 1.5 s]: the MPPT control is enabled to provide the maximum active power with the unity power factor.
- Interval 2 [from 1.5 s to 2.5 s]: the PQ control is activated, the demanded active power is set to 2 MW ($P_{wf}^{ref} = 2$ MW). At time $t = 3$ s, a disconnection of the third wind turbine ocured.
- Interval 3 [from 2.5 s to 3 s]: the MPPT control is selected.
- Interval 4 [from 3 s to 4 s]: the PQ control is activated. The required active power is equal to 3 MW, for the reactive power from 3 s to 3.5 s, the WF consumes 2.4 MVAR and it generates a reactive power of 4 MVAR at 3.5 s to 4 s.
- Interval 5 [from 4 s to 5 s]: the MPPT control is selected.

Disconnection of the WT_3 turbine leads to a reduction in the reactive power of the wind

farm Fig. 16(d). However the powers produced by the farm still follow their references Fig. 16(a). This is due to the fact that the two other wind turbines produce more power to make up the missing power as shown in Fig. 16(b) and Fig. 16(c). On the other hand, at time 3.5 s, the transmission system operator demanders a reactive power generation (4 MVAR), but the wind farm cannot meet this demand because it's greater than its maximum value. For this and according to the algorithm in Appendix 1.2. , the WF generates the available maximum reactive power.

Figure 17 demonstrates that the reactive power of WTs supplied by the stators is more than sufficient to satisfy the reactive power demand of the wind farm from $t = 3$ s to $t = 3.5$ s. When the grid demand for reactive power increases to 4 MVA from $t = 3.5$ s to $t = 4$ s, the windings of the stator of the WTs are not capable of handling this request and they make their GSCs contribute to the reactive power generation. This is proportionally distributed over all 3 WTs without exceeding the boundaries of their corresponding converters.

7.3. Test3: Voltage Support Under Grid Faults

In this test, we have activated the three operating modes for the production of maximum active power capacity and the respect of the requested power from the TSO. The other other aim in this test consist also in checking the LVRT capability in accordance with the German GC requirements for the voltage support under grid faults. Further, the electrical power network is placed under asymmetrical voltage drop with a depth of 40 % and duration of 500 ms as shown in Fig. 18. The test scenario is defined as follows:

- Interval 1: From 0 s to 1.5 s, the MPPT mode is selected to achieve maximum production and guarantee a unitary power factor at PCC.
- Interval 2: From 1.5 s to 2.5 s. The TSO demander the required active power equal to 3 MW ($P_{wf}^{ref} = 3$ MW), and for the required reactive power from 1.5 s to 2 s, the WF can consumes 2.4 MVAR. In contrast from 2 s to 2.5 s, it generates reactive power equal to 2.4 MVAR (PQ control).
- Interval 3: From 2.5 s to 3.5 s, the MPPT control is selected.
- Interval 4: The fault control is activated from 3.5 s to 4 s, with a balanced fault that leads the voltage at PCC to drop to 40 % within 500 ms.
- Interval 5: From 4 s to 5 s, the MPPT control is selected.

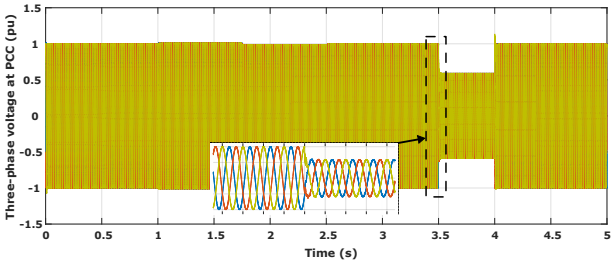

Fig. 18: Three phase voltage at PCC.

The grid voltage and the electrical angular speed at PCC are shown in Fig. 19.

From Fig. 20, it can be seen that on behalf of the optimal (MPPT) control the active power produced by the WF at PCC is the summation of the optimal active powers of the three WGs, and the reactive power at PCC is set to zero (Fig. 20(a)). This is because the farm reacts with the predetermined active and reactive powers by the TSO (PQ control). However, when a grid fault causing a voltage drop of 40 % occurs, it automatically activates the LVRT control (fault control). Therefore, in order to ensure the voltage support under grid faults in accordance with the GCRs, the wind turbines participate by injecting the reactive power which is proportional to the gird voltage drop as observed in Fig. 20(b), Fig. 20(c) and Fig. 20(d).

Finally, based on all the simulation results presented in this paper, it can be concluded that the combination of the supervisory system based on the PD algorithm and the suggested ADRC approach is sufficiently strong, robust, and guarantees better performances in terms of reactive and active powers monitoring of the wind farms at PCC, and on the other hand, in contributing to the voltage stability and security while respecting the grid code requirements.

8. Conclusion

In this paper, we have presented a new management and monitoring control strategies of reactive and active powers for a DFIG-based large-scale WF. This control handles the power generation of the entire WF at the PCC based on the current state of the grid and the requested control mode, and dispatches the power generation between the stator circuit and the grid side converter. Moreover, in order to ensure that each WT of the farm operates far enough away from its maximum energy production capacity while using the supervision system based on the PD algorithm.

A new robust control strategy for the WT is suggested, which combines the Linear ADRC approach and the LVRT control strategy. Therefore, there are three operating modes of WT control. The MPPT control mode is responsible for injecting the maximum

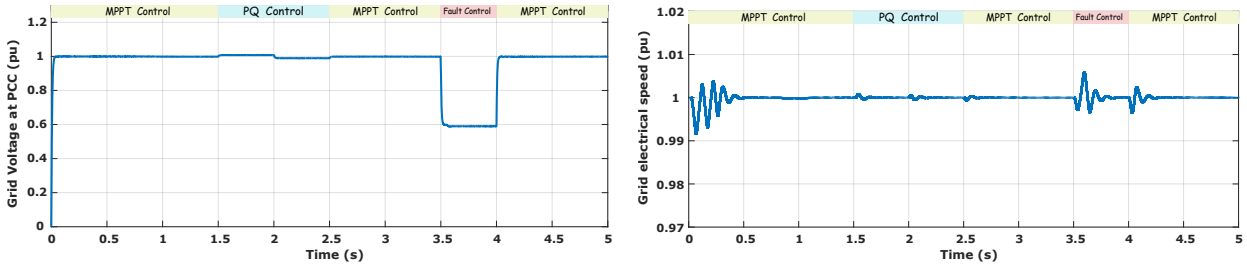

(a) (b)

Fig. 19: Simulation results of test 3: (a) Grid voltage with 40 % dip, (b) Electrical angular speed.

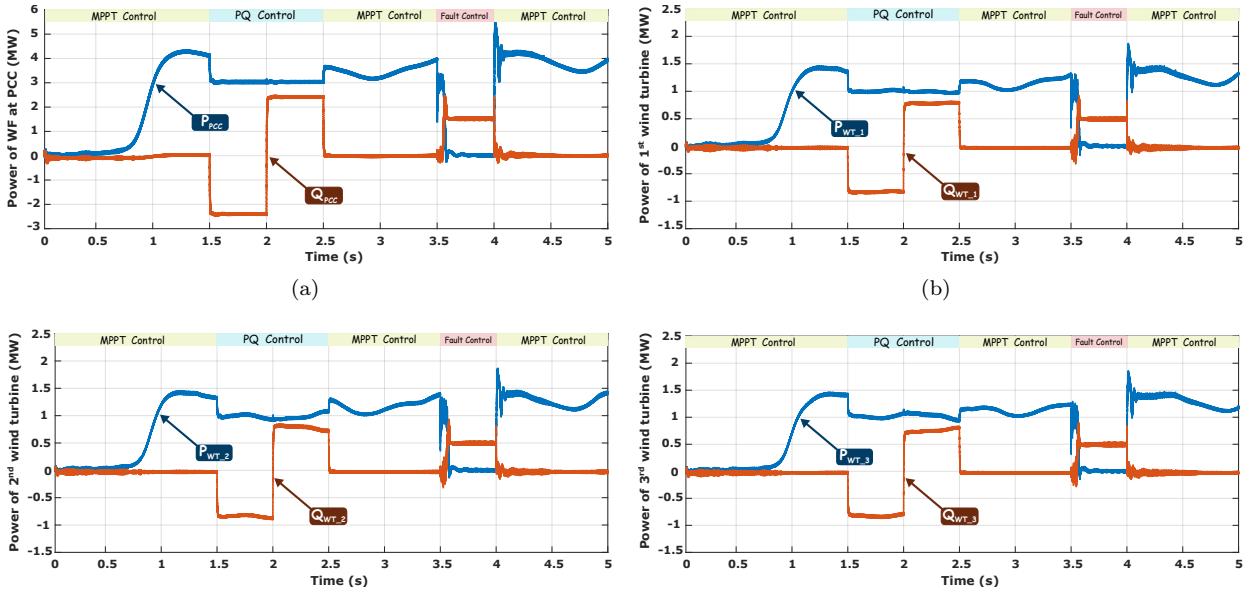

(a) (b)

(c) (d)

Fig. 20: Simulation results of test 3 (P_i,Q_i): (a) of the wind farm, (b) of the 1^{st} wind turbine, (c) of the 2^{nd} wind turbine, (d) of the 3^{rd} wind turbine.

power and the PCC reactive power control. The PQ mode is used to meet the demand of reactive and active powers specified by the TSO, and finally, the fault mode is enabled once a grid fault condition is occurred using the voltage control method to meet the GC requirements.

The results obtained confirm the effectiveness of the control approach to decoupled control of the active and reactive powers for any kind of operating mode. And they showed that the supervisory control system of the wind farm based on the ADRC strategy confirms, the effectiveness of the WF active and reactive power control to meet the TSO demands, and to overcome the grid faults while injecting the required reactive power according to the German GC requirements.

References

[1] Renewables 2016 Global Status Report. In: *REN21* [Online]. 2017. Available at: `https://www.ren21.net/wp-content/uploads/2019/05/REN21_GSR2016_FullReport_en_11.pdf`.

[2] BLAABJERG, F. and K. MA. Wind energy systems. *Proceedings of the IEEE*. 2017. vol. 105, iss. 11, pp. 2116–2131. ISSN 1558-2256. DOI: 10.1109/JPROC.2017.2695485.

[3] DIESENDORF, M. and B. ELLISTON. The feasibility of 100% renewable electricity systems: A response to critics. *Renewable and Sustainable Energy Reviews*. 2018, vol. 93, iss. 1. pp. 318–330. ISSN 1879-0690. DOI: 10.1016/j.rser.2018.05.042.

[4] ZIAEI, A., R. GHAZI and R. Z. DAVARANI. Linear Modal Analysis of Doubly-Fed Induction

Generator (DFIG) Torsional Interaction: Effect of DFIG Controllers and System Parameters. *Advances in Electrical and Electronic Engineering*. 2018, vol. 16, iss. 4, pp. 388–401. ISSN 1804-3119. DOI: 10.15598/aeee.v16i4.2265.

[5] LAGHRIDAT, H., A. ESSADKI and T. NASSER. Comparative Analysis between PI and Linear-ADRC Control of a Grid Connected Variable Speed Wind Energy Conversion System Based on a Squirrel Cage Induction Generator. *Mathematical Problems in Engineering*. 2019, vol. 2019. iss. 1, pp. 1–16. ISSN 1563-5147. DOI: 10.1155/2019/8527183.

[6] ABOUDRAR, I., S. E. H. SOUMIA, H. MEDIOUNI and A. AGHMADI. Modeling and Robust Control of a Grid Connected Direct Driven PMSG Wind Turbine By ADRC. *Advances in Electrical and Electronic Engineering*. 2018, vol. 16, iss. 4, pp. 402–413. ISSN 1804-3119. DOI: 10.15598/aeee.v16i4.2952.

[7] NADOUR, M., A. ESSADKI and T. NASSER. Improving low-voltage ride-through capability of a multimegawatt DFIG based wind turbine under grid faults. *Protection and Control of Modern Power Systems*. 2020, vol. 5, iss. 1, pp. 1–13. ISSN 2367-0983. DOI: 10.1186/s41601-020-00172-w.

[8] TAPIA, G., A. TAPIA and J. X. OSTOLAZA. Proportional–Integral Regulator-Based Approach to Wind Farm Reactive Power Management for Secondary Voltage Control. *IEEE Transactions on Energy Conversion*. 2007, vol. 22, iss. 2, pp. 488–498. ISSN 1558-0059. DOI: 10.1109/TEC.2005.858058.

[9] FORTMANN, J., M. WILCH, F. KOCH and I. ERLICH. A novel centralised wind farm controller utilising voltage control capability of wind turbines. In: *16th Power Systems Computation Conference (PSCC)*. Glasgow: PSCC, 2008, pp. 1–7. ISBN 978-1-6173-8857-6.

[10] RODRIGUEZ-AMENEDO, J. L., S. ARNALTE and J. C. BURGOS. Automatic generation control of a wind farm with variable speed wind turbines. *IEEE Transactions on energy conversion*. 2002, vol. 17, iss. 2, pp. 279–284. ISSN 1558-0059. DOI: 10.1109/TEC.2002.1009481.

[11] BENLAHBIB, B., N. BOUARROUDJ, F. BOUCHAFAA and B. BATOUN. Fractional Order PI Controller for wind farm supervision. In: *2014 IEEE International Conference on Industrial Engineering and Engineering Management*. Selangor: IEEE, 2014, pp. 1234–1238. ISBN 978-1-4799-6410-9. DOI: 10.1109/IEEM.2014.7058835.

[12] JUNG, S and G. JANG. A Loss Minimization Method on a Reactive Power Supply Process for Wind Farm. *IEEE Transactions on Power Systems*. 2017, vol. 32, iss. 4, pp. 3060–3068. ISSN 1879-3517. DOI: 0.1016/j.ijepes.2015.01.021.

[13] KANNA, B. and S. N. SINGH. Towards reactive power dispatch within a wind farm using hybrid PSO. *International Journal of Electrical Power & Energy Systems*. 2015, vol. 69, iss. 1, pp. 232–40. ISSN 1558-0679. DOI: 10.1109/TPWRS.2016.2621162.

[14] ZHANG, B, P. HOU, W. HU, M. SOLTANI, C. CHEN and Z. CHEN. A Reactive Power Dispatch Strategy With Loss Minimization for a DFIG-Based Wind Farm. *IEEE Trans Sustain Energy*. 2016, vol. 7, iss. 3, pp. 914–923. ISSN 1949-3037. DOI: 10.1109/TSTE.2015.2509647.

[15] MERAHI, F., El. M. BERKOUK and S. MEKHILEF. New management structure of active and reactive power of a large wind farm based on multilevel converter. *Renewable energy*. 2014, vol. 68, iss. 3, pp. 814–828. ISSN 1879-0682. DOI: 10.1016/j.renene.2014.03.007.

[16] ELYAALAOUI, K., M. OUASSAID and M. CHERKAOUI. Dispatching and control of active and reactive power for a wind Farm considering fault ride-through with a proposed PI reactive power control. *Renewable Energy Focus*. 2019, vol. 28, pp. 56–65. ISSN 1878-0229. DOI: 10.1016/j.ref.2018.11.002.

[17] LAGHRIDAT, H., A. ESSADKI, M. ANNOUKOUBI and T. NASSER. A Novel Adaptive Active Disturbance Rejection Control Strategy to Improve the Stability and Robustness for a Wind Turbine Using a Doubly Fed Induction Generator. *Journal of Electrical and Computer Engineering*. 2020, vol. 2020, iss. 1, pp. 1–14. ISSN 2090-0147. DOI: 10.1155/2020/9847628.

[18] YANG, J., J. E. FLETCHER and J. O'REILLY. A Series-Dynamic-Resistor-Based Converter Protection Scheme for Doubly-Fed Induction Generator During Various Fault Conditions. *IEEE Transactions on Energy Conversion*. 2010, vol. 25, iss. 2, pp. 422–432. ISSN 1558-0059. DOI: 10.1109/TEC.2009.2037970.

[19] JUSTO, J. J. and R. C. BANSAL. Parallel R-L configuration crowbar with series R-L circuit protection for LVRT strategy of

DFIG under transient-state. *Electric Power Systems Research*. 2018, vol. 154, iss. 1, pp. 299–310. ISSN 1873-2046. DOI: 10.1016/j.epsr.2017.09.002.

[20] PANNELL, G., B. ZAHAWI, D. J. ATKINSON and P. MISSAILIDIS. Evaluation of the Performance of a DC-Link Brake Chopper as a DFIG Low-Voltage Fault-Ride-Through Device. *IEEE Transactions on Energy Conversion*. 2013, vol. 28, iss. 3, pp. 535–542. ISSN 1558-0059. DOI: 10.1109/TEC.2013.2261301.

[21] HUCHEL, L., M. S. E. MOURSI and H. H. ZEINELDIN. A Parallel Capacitor Control Strategy for Enhanced FRT Capability of DFIG. *IEEE Transactions on Sustainable Energy*. 2014, vol. 6, iss. 2, pp. 303–312. ISSN 1949-3037. DOI: 10.1109/TSTE.2014.2371925.

[22] GKAVANOUDIS, S. I. and C. S. DEMOULIAS. Fault ride-through capability of a DFIG in isolated grids employing DVR and supercapacitor energy storage. *International Journal of Electrical Power & Energy Systems*. 2015, vol. 68, iss. 1, pp. 356–363. ISSN 1879-3517. DOI: 10.1016/j.ijepes.2014.12.068.

[23] GHOSH, S. and S. KAMALASADAN. An Energy Function-Based Optimal Control Strategy for Output Stabilization of Integrated DFIG-Flywheel Energy Storage System. *IEEE Transactions on Smart Grid*. 2016, vol. 8, iss. 4, pp. 1922–1931. ISSN 1949-3061. DOI: 10.1109/TSG.2015.2510866.

[24] EL-HELW, H. and A. KHALED. Comparison study between two Dynamic Breaking resistor techniques in protecting the doubly fed induction generator. In: *2013 12th International Conference on Environment and Electrical Engineering*. Wroclaw: IEEE, 2013, pp. 25–29. ISBN 978-1-4673-3059-6. DOI: 10.1109/EEEIC.2013.6549535.

[25] NDERI, S. B., M. NEGNEVISTKY, A. JALILIAN and M. T. HAGH. Non-controlled fault current limiter to improve fault ride through capability of DFIG-based wind turbine. In: *2016 IEEE Power and Energy Society General Meeting (PESGM)*. Boston: IEEE, 2016, pp.1–5. ISBN 978-1-5090-4168-8. DOI: 10.1109/PESGM.2016.7741624.

[26] ELSHIEKH, M. E., D.-E. A. MANSOUR and A. M. MZMY. Improving Fault Ride-Through Capability of DFIG-Based Wind Turbine Using Superconducting Fault Current Limiter. *IEEE Transactions on Applied Superconductivity*. 2012, vol. 23, iss. 3, pp. 5601204–5601204. ISSN 1558-2515. DOI: 10.1109/TASC.2012.2235132.

[27] MOHAMMED, E. M. and G. JOOS. Optimal tracking secondary voltage control for the DFIG wind turbines and compensator devices. *Electric power systems research*. 2009, vol. 79, iss. 12, pp. 1705–1716. ISSN 1873-2046. DOI: 10.1016/j.epsr.2009.07.009.

[28] EL-MOURSI, M. S. Fault ride through capability enhancement for self-excited induction generator-based wind parks by installing fault current limiters. *IET renewable power generation*. 2011, vol. 5, iss. 4, pp. 269–280. ISSN 1752-1424. DOI: 10.1049/iet-rpg.2010.0123.

[29] JERIN, A. R. A., P. KALIANNAN and U. SUBRAMANIAM. Improved fault ride through capability of DFIG based wind turbines using synchronous reference frame control based dynamic voltage restorer. *ISA Transactions*. 2017, vol. 70, iss. 4, pp. 465-474. ISSN 1879-2022. DOI: 10.1016/j.isatra.2017.06.029.

[30] YANG, R.-H. and J. X JIN. Unified Power Quality Conditioner with Advanced Dual Control for Performance Improvement of DFIG-based Wind Farm. *IEEE Transactions on Sustainable Energy*. 2020, vol. 12, iss. 1, pp. 116–126. ISSN 1557-9948. DOI: 10.1109/41.720325.

[31] KAZMIERKOWSKI, M. P. and L. MALESANI. Current control techniques for three-phase voltage-source PWM converters: A survey. *IEEE Transactions on Industrial Electronics*. 1998, vol. 45, iss. 5, pp. 691–703. ISSN 1949-3037. DOI: 10.1109/TSTE.2020.2985161.

[32] MOHSENI, M., S. M. ISLAM and M. A. S. MASOUM. Enhanced Hysteresis-Based Current Regulators in Vector Control of DFIG Wind Turbines. *IEEE Transactions on Power Electronics*. 2010, vol. 26, iss. 1, pp. 223–234. ISSN 941-0107. DOI: 10.1109/TPEL.2010.2058816.

[33] LIANG, J., W. QIAO, and R. HARLEY and G. Ronald. Feed-Forward Transient Current Control for Low-Voltage Ride-Through Enhancement of DFIG Wind Turbines. *IEEE Transactions on Energy Conversion*. 2010, vol. 25, iss. 3, pp. 836–843. ISSN 1558-0059. DOI: 10.1109/TEC.2010.2048033.

[34] KAMEL, R. M. Three fault ride through controllers for wind systems running in isolated micro-grid and Effects of fault type on their performance: A review and comparative study. *Renewable and Sustainable Energy Reviews*. 2014, vol. 37, iss. 1, pp. 698-714. ISSN 1879-0690. DOI: 10.1016/j.rser.2014.05.065.

[35] BENBOUZID, M., B. BELTRAN, Y. AMIRAT. G. YAO, J. HAN and H. MANGELA. Second-order sliding mode control for DFIG-based wind turbines fault ride-through capability enhancement. *ISA Transactions*. 2014, vol. 53, iss. 3, pp. 827–833. ISSN 1879-2022. DOI: 10.1016/j.isatra.2014.01.006.

[36] MENSOU, S., A. ESSADKI, T. NASSER and B. B. IDRISSI. A direct power control of a DFIG based-WECS during symmetrical voltage dips. *Protection and Control of Modern Power Systems*. 2020, vol. 5, iss. 1, pp. 1–12. ISSN 2367-0983. DOI: 10.1186/s41601-019-0148-y.

[37] YASSIN, H. M., H. H. HANAFY and M. M. HALLOUDA. Enhancement low-voltage ride through capability of permanent magnet synchronous generator-based wind turbines using interval type-2 fuzzy control. *IET Renewable Power Generation*. 2016, vol. 10, iss. 3, pp. 339–348. ISSN 1752-1424. DOI: 10.1049/iet-rpg.2014.0453.

[38] CALLE-PRADO, A., S. ALEPUZ, J. BORDONAU, J. NICOLAS-APRUZZESE, P. CORTES and J. RODRIGUEZ. Model Predictive Current Control of Grid-Connected Neutral-Point-Clamped Converters to Meet Low-Voltage Ride-Through Requirements. *IEEE Transactions on Industrial Electronics*. 2014, vol. 62, iss. 3, pp. 1503–1514. ISSN 1557-9948. DOI: 10.1109/TIE.2014.2364459.

[39] MOHSENI, M and S. M. ISLAM. Review of international grid codes for wind power integration: Diversity, technology and a case for global standard. *Renewable and Sustainable Energy Reviews*. 2012, vol. 16, iss. 6, pp. 3876–3890. ISSN 1879-0690. DOI: 10.1016/j.rser.2012.03.039.

[40] TOHIDI, S. and B. MOHAMMADI-IVATLOO. A comprehensive review of low voltage ride through of doubly fed induction wind generators. *Renewable and Sustainable Energy Reviews*. 2016, vol. 57, iss. 1, pp. 412–419. ISSN 1879-0690. DOI: 10.1016/j.rser.2015.12.155.

[41] LAZRAK, A. and A. ABBOU. H_∞ Control of Wrim Driven Flywheel Storage System to Ride-Through Grid Voltage Dips. *Advances in Electrical and Electronic Engineering*. 2020, vol. 18, iss. 1, pp. 11–22. ISSN 1804-3119. DOI: 10.15598/aeee.v18i1.3546.

[42] HAN, J. From PID to Active Disturbance Rejection Control. *IEEE Transactions on Industrial Electronics*. 2009, vol. 56, iss. 3, pp. 1900–906. ISSN 1557-9948. DOI: 10.1109/TIE.2008.2011621.

[43] HUANG, Y. and W. XUE. Active disturbance rejection control: methodology and theoretical analysis. *ISA transactions*. 2014, vol. 53, iss. 4, pp. 963–976. ISSN 1879-2022. DOI: 10.1016/j.isatra.2014.03.003.

[44] MA, Y., L. YANG, X. ZHOU, X. YANG, Y. ZHOU and B. ZHANG. Linear Active Disturbance Rejection Control for DC Bus Voltage Under Low-Voltage Ride-Through at the Grid-Side of Energy Storage System. *Energies*. 2020, vol. 13, iss. 5, pp. 1–22. ISSN 1996-1073. DOI: 10.3390/en13051207.

[45] HERBST, G. A Simulative Study on Active Disturbance Rejection Control (ADRC) as a Control Tool for Practitioners. *Electronics*. 2021, vol. 2, iss. 3, pp. 246–279. ISSN 2079-9292. DOI: 10.3390/electronics2030246.

[46] HERBST, G. Practical Active Disturbance Rejection Control: Bumpless Transfer, Rate Limitation, and Incremental Algorithm. *IEEE Transactions on Industrial Electronics*. 2016, vol. 63, iss. 3, pp. 1754–1762. ISSN 1557-9948. DOI: 10.1109/TIE.2015.2499168.

[47] RAN, M, Q. WANG, C. DONG and L. XIE. Active disturbance rejection control for uncertain time-delay nonlinear systems. *Automatica*. 2020, vol. 112, iss. 1, pp. 1–9. ISSN 1873-2836. DOI: 10.1016/j.automatica.2019.108692.

[48] CHU, Z. *Active disturbance rejection control: applications, stability analysis, and tuning method*. Winnipeg, 2018. Dissertation. The University of Manitoba. Supervisor Dr. Christine Wu.

[49] FU, C. and W. TAN. Tuning of linear ADRC with known plant information. *ISA Transactions*. 2016, vol. 65, iss. 1, pp. 384–393. ISSN 1879-2022. DOI: 10.1016/j.isatra.2016.06.016.

[50] GHENNAM, T., K. ALIOUANE, F. AKEL, B. FRANCOIS and E. M. BERKOUK. Advanced control system of DFIG based wind generators for reactive power production and integration in a wind farm dispatching. *Energy Conversion and Management*. 2015, vol. 105, iss. 1, pp. 240–250. ISSN 1879-2227. DOI: 10.1016/j.enconman.2015.07.058.

[51] LAGHRIDAT, H., A. ESSADKIL, M. ANNOUKOUBIL and T. NASSER. Linear Active Disturbance Rejection Control (LADRC) of a Variable Speed Wind Energy Conversion System using a DFI-Generator. In: *2018 6th International Renewable and Sustainable Energy Conference (IRSEC)*. Rabat: IEEE, 2018, pp. 1–6. ISBN 978-1-7281-1182-7. DOI: 10.1109/IRSEC.2018.8703027.

[52] KO, H.-S., G.-G. YOON, N.-H. KYUNG and W.-P. HONG. Modeling and control of DFIG-based variable-speed wind-turbine. *Electric Power Systems Research*. 2008, vol. 78, iss. 11, pp. 1841–1849. ISSN 1873-2046. DOI: 10.1016/j.epsr.2008.02.018.

[53] BRANDAO, D. I., F. E. G. MENDES, R. V. FERREIRA, S. M. SILVA and I. A. PIRES. Active and Reactive Power Injection Strategies for Three-Phase Four-Wire Inverters During Symmetrical/Asymmetrical Voltage Sags. *IEEE Transactions on Industry Applications*. 2019, vol. 55, iss. 3, pp. 2347–2355. ISSN 1939-9367. DOI: 10.1109/TIA.2019.2893135.

[54] MAHELA, O. P., N. GUPTA, M. KHOSRAVY and N. PATEL. Comprehensive Overview of Low Voltage Ride Through Methods of Grid Integrated Wind Generator. *IEEE Access*. 2019, vol. 7, iss. 1, pp. 99299–99326. ISSN 2169-3536. DOI: 10.1109/ACCESS.2019.2930413.

Appendix A

1.1. Appendix-1

The DFIG-based wind turbine system parameters used for the validation of simulation are given in the Tab. 1, Tab. 2 and Tab. 3 [54].

Tab. 1: Turbine-parameters.

Symbols	Parameters	Values
P_m	Mechanical Power	1.5 MW
R	Blade radius	31 m
w	Nominal wind speed	12 m·s^{-1}
G	Gearbox ratio	59
ρ	Density of Air	1.225 kg·m^{-3}

Tab. 2: DFIG-parameters.

Symb.	Parameters	Values
P_{wg_n}	Nominal Active Power	1.5 MW
U_n	Rated Voltage	690 V
f_n	Nominal Frequency	50 Hz
N_n	Rated Rotor Speed	1750 tr·min^{-1}
p	Pole Pairs Number	2
R_r	Rotor Resistance	2.63 mΩ
R_s	Stator Resistance	2.65 mΩ
L_m	Magnetizing Inductance	5.4749 mH
$L_{r\sigma}$	Rotor Inductance	0.1337 mH
$L_{s\sigma}$	Stator Inductance	0.1687 mH

Tab. 3: Grid-Side parameters.

Symbols	Parameters	Values
C	DC-Bus Cpacitor	10028.17 µF
V_{dc}	DC-Bus Voltage	1320 V
L_f	Filter Inductancer	1.0103 mH
R_f	Filter Resistance	0.3174 Ω

1.2. Appendix-2

The supervisory algorithm which manages the active and reactive powers of a DFIG-based wind farm is summary in the following Fig. 21.

List of Abbreviations

RES	Renewable Energy Sources,
WFs	Wind Farms,
PMSG	Permanent Magnet Synchronous Generator,
WTs	Wind Turbines,
SCIG	Squirrel Cage Induction Generator,
TSO	Transmission System Operator ,
DFIG	Doubly Fed Induction Generator,
CSU	Central Supervision Unit,
LSU	Local Supervision Unit,
LVRT	Low Voltage Ride Through,
GCR	Grid Code Requirement,
PD	Proportional Distribution,
PI	Proportional Integral,
ADRC	Active Disturbance Rejection Control,
OF	Optimization Functions,
NLSEF	Non-Linear Sate Error Feedback,
LADRC	Linear Active Disturbance Rejection Control,
ESO	Extended State Observer,
TD	Tracking Differentiator,
PLL	Phase-Locked Loop,
WECS	Wind-Europe's Central Scenario,
MPPT	Maximum Power Point Tracking,
GSC	Grid-Side Converter,
PCC	Point of Common Coupling,
RSC	Rotor-Side Converter.

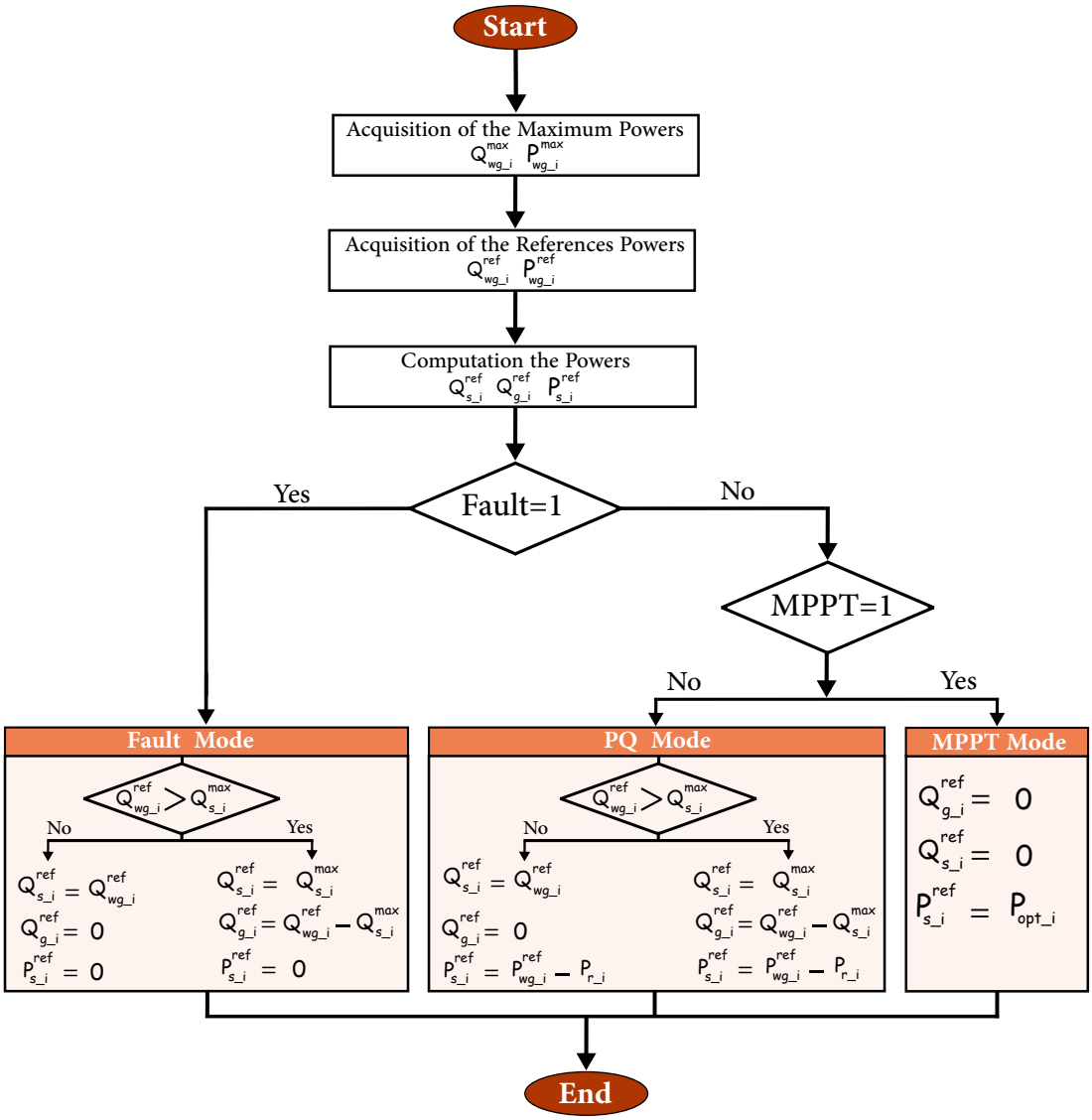

Fig. 21: Local management algorithm of Powers WTs.